Klamath/San Joaquin/Sacramento
Hydroclimatic Reconstructions from Tree Rings

August 15, 2014

David M. Meko, Connie A. Woodhouse, and Ramzi Touchan

Final Report to California Department of Water Resources

Agreement 4600008850

Contents

List of Tables

List of Figures

1.Introduction

This is a draft final report for Agreement Number 4600008850, "Klamath/San Joaquin/Sacramento Hydroclimatic Reconstructions", signed October 13, 2010. Following an extension, signed on May 28, 2013, the contract end date is June 30, 2014. Work includes developing new and updated tree-ring chronologies, reconstructing specified streamflow and/or precipitation records in the Klamath, San Joaquin and Sacramento River Basins, and analyzing the time series properties of the reconstructions. These reconstructions allow assessment of hydrologic variability over centuries to millennia and give context for assessing recent drought events.

Tasks on this project included field collections; laboratory work in sample preparation, dating and measurement; and statistical work in chronology development, reconstruction, and analysis of those reconstructions. The interpretation of the reconstructions includes five main components : 1) place instrumental-period flow statistics in a long-term context, 2) quantify droughts and wet periods, 3) identify cycles in wetness and dryness, 4) check consistency with other paleoclimatic data, and 5) assess reconstructed flow variations in the context of expected scenarios of climate. A total of 16 different hydroclimatic series – 11 flow records and 5 precipitation records, were reconstructed.

This report summarizes the research project products and results. The Data and Methods section of this report describes the field collections and development of tree-ring chronologies, reconstruction modeling, and methods of analyzing reconstructions. The Results section focuses on the interpretation of selected key reconstructions for the Klamath, Sacramento, and San Joaquin basins. Annual time series of the 16 reconstructions are included as products in an appendix and in a digital spreadsheet.

2. Data and Methods

Field collection, chronology development and statistical conversion of chronologies into reconstructed time series of flow or precipitation were done separately by two different research teams for the Klamath (Woodhouse/Malevich) and Sacramento/San Joaquin Basins (Meko/Touchan). Analyses of reconstructions were conducted with the same methods for both sets of basins. The following sections accordingly are subdivided, with separate parts for the Klamath and Sacramento/San Joaquin for Field Collections and Chronology Development and Reconstruction, and one part for Analysis of Reconstructions.

2.1 Field Collections and Chronology Development—Klamath Basin

Field Collections. We updated 12 existing collections and made five new collections in southeastern Oregon and northeastern California. Re-collection sites were identified based on the strength of correlations between pre-existing tree-ring data and flow or precipitation records to be used in the reconstruction models. In addition to the five collections made in the fall of 2010, 12 collections were made in July, 2011. Site information, along with information on tree-species, number of samples, and time coverage are listed in Table 1. Site locations are shown on the map in Figure 1. Two of the new collections found to be too young to be useful so were not developed into chronologies, and are not included in the table or figure.

Chronology Development. These main steps were followed for chronology generation: 1) cross-dating by skeleton plot (Stokes and Smiley 1968), 2) ring measurement using a Velmex sliding stage, 3) quality control on dating using COFECHA (Holmes 1983), 4) quality check and/or reassessment/re-measurement of wood as necessary, and 5) computation of site chronology by the ratio method using R (dplR package, Bunn 2010). After chronologies were developed, the wood samples with unequivocal dating were pin-pricked for archiving such that the dating is hard-coded onto the samples.

For updated chronologies, a subset of samples from previous collections was combined with the new samples. To maintain the length of the original chronologies, ten of the longest tree samples from the original site collections were combined with the updated collection. Samples from the original collections were also chosen to maintain an adequate sample depth (i.e., number of samples). We used the criterion of Expressed Population Signal (EPS) of at least 0.85 (Wigley et al. 1984) to judge whether the sample size is adequate.

Measured tree-ring series were detrended using a 67%N spline, defined as a cubic spline with a frequency response of 0.5 at two-thirds the length of the series (Cook and Peters 1981). Low-lag persistence, when present, was removed from the detrended series by fitting an auto-regressive model with order selected for minimum Akaike Information Criterion (AIC) (Akaike 1974, Box et al. 1994) to generate residual chronologies. Standard chronologies, in which low-order persistence was not removed, were also retained. Tukey's biweight robust mean was used to average the measured, detrended series into both standard and residual site chronologies.

2.2 Field Collections and Chronology Development – Sacramento/San Joaquin Basins

Field Collections. Field collections of tree-ring data were made at 14 different sites for the Sacramento/San Joaquin part of the study between August 2011 and November 2013. Core samples were taken on four trips, and both cores and cross-sections (chainsaw) on one trip. Previous experience with sampling for hydrologic studies in the region (Meko et al. 2001) was used as a guide for site and species selection. Sites collected, along with information on tree-species, number of samples, and time coverage are listed in Table 1. Site locations are shown on the map in Figure 1. All except one site collected is from the Sierra Nevada. The exception is site #26, a *Quercus douglasii* (blue oak), selected for updating because of its demonstrably strong precipitation regional precipitation signal (Meko et al. 2011). Eight of the 14 sites visited were updates aimed a bringing chronologies to present and/or increasing the sample depth in earlier centuries. Six of the sites are new collections.

Chronology Development. Initial steps in chronology development were the same as described above for the Klamath Basin. Measured ring widths were then standardized, or converted to site chronologies, by Matlab tree-ring standardization functions treeprep and treetrim following steps described in Meko et al. (2007) in reconstruction of Colorado River flows. Growth trend was described by fitting a cubic smoothing spline (Cook and Peters 1981) with frequency response 0.95 at twice the series length to each ring-width series, and then was removed by computing core indices as the ratio of measured ring width to the value of the fitted curve in each year. A spline with the identical specifications was then applied to the absolute departures of core indices from their long-term mean to remove trend in variance in the individual core indices (e.g., Meko et al., 1993). The site chronology was then computed as the biweight mean of the core indices available in each year if the sample size is less than six cores, and otherwise by the median of the core indices. Finally, variance-stabilization, following Osborn et al. (1997), was applied to the site chronology to adjust for possible temporal changes of chronology variance associated with changing sample size (number of cores) over time.

2.3 Reconstruction – Klamath Basin

Reconstruction models were developed for

- Klamath River at Keno OR (water year, estimated natural flow, U.S. Bureau of Reclamation, via Maury Roos)
- Trinity River at Lewiston CA (water year streamflow, estimated natural flow, CADWR)

- Klamath Falls climate station (water year precipitation, NOAA's U.S. Historical Climate Network)
- Yreka climate stations (water year precipitation, NOAA's U.S. Historical Climate Network)
- Weaverville climate stations (water year precipitation, NOAA's U.S. Historical Climate Network)

For Klamath Falls precipitation, two reconstruction models were developed using stepwise multiple linear regression. The first of these models was designed to emphasize high model skill (covering 1610 - 2004). The second was designed to emphasize reconstruction length (covering 1000 - 2010). The pool of candidate chronologies for these reconstructions included 10 chronologies from this study and seven moisture-sensitive chronologies from the International Tree-Ring Databank (ITRDB). ITRDB chronologies selected started in 1650 or before, ended in 1996 or later, and were of species known to be sensitive to moisture. The pool was based on residual chronologies that were significantly correlated ($p< 0.05$) with the Klamath Falls precipitation record. Leave-one-out cross-validation (Michaelsen et al. 1987) was used to validate these reconstructions. The final shorter model explains 59% of the total variance (using seven chronologies) and the longer model explains 53% of the variance (using three of the chronologies). The Klamath Falls precipitation reconstructions have been published in the *Journal of Hydrology* (Malevich et al. 2013).

The Trinity River streamflow and Yreka and Weaverville water year precipitation reconstructions were developed using the same methodology as above, with two differences. First, only one reconstruction model was developed for each record. Second, a larger number of chronologies from the ITRDB was used in the pool of candidate chronologies (from a slightly larger geographic area), again based on significant correlations with the instrumental record, for a total of twenty chronologies in the pool for stepwise regression.

A preliminary reconstruction of the Klamath River at Keno streamflow reconstruction was also developed using stepwise regression. This reconstruction was calibrated on the estimated natural flows developed by the Bureau of Reclamation. Because there is uncertainty about the accuracy of the natural flow estimates, we consider this to be a preliminary reconstruction (see information on sensitivity testing at the end of this section). The reconstruction approach was used as is described for the Trinity River flow, and Weaverville and Yreka precipitation above. A second approach to try to account significant low order persistence (that is, a carry- over effect from one year to the next several years), both the set of chronologies (the standard chronologies, in this case) in the predictor pool and the calibration data (streamflow series) were pre-whitened (the persistence was removed) using autoregressive (AR) modeling over the calibration period. The AR models from the calibration period were then fit to the full length chronologies. The pre-whitened chronologies were screened for common end date of at least 2000, and significant correlation ($p < 0.05$) with the gage record. The regression model was then fit using all years for the calibration data (1949-2000). The full length reconstruction was generated with the pre-whitened chronologies, and then persistence was restored to the reconstructed streamflow series using AR equation initially used to prewhiten the series. Since this approach did not appreciably improve the persistence, the initial reconstruction approach was used for this report.

For all of the above reconstructions, 50% confidence intervals were calculated from the RMSE statistic for each model calibration in the cross validation process.

The reconstruction skill for the Klamath models, based on the model calibration, is shown in terms of the variance explained by the reconstruction model (R^2 and R^2 adjusted for the number of predictors in the model, in Table 2, top). The validations statistics for each model (reduction of error, RE, and the root mean squared error) reflect the skill of the reconstruction model when assessed on data withheld from the calibration. In the Klamath basin reconstruction, the model skill for the precipitation reconstructions is slightly lower than for the flow reconstructions. Water-year streamflow is a measure that integrates over space (the watershed) and time (the water year). It also integrates several climatic factors; precipitation mostly but also temperature, and to a lesser degree relative humidity and wind. The net result of these factors over the course of the water year is the annual flow. Tree growth in this region

is also integrating the combined influence of a very similar set of climate variables over the water year. In contrast, the precipitation reconstructions are based on a record that is for a single point and for one variable, and thus, these reconstruction are slightly less skillful (54-60% variance explained versus 63-68% variance explained).

We have recently extended the work on the Klamath River at Keno to include testing sensitivity of the reconstruction to uncertainty in the estimated natural flows used to calibrate the reconstruction described above. In work still in progress, we are exploring the nature of the uncertainty in the gaged flows using an approach that assesses the differences between inflows (Williamson and Sprague Rivers) into Upper Klamath Lake and natural flows estimated for the USGS gage, Klamath at Keno (below Upper Klamath Lake). In doing so, we acknowledge that there is no perfect record of natural flow for this gage, but make an assumption that a likely range of values falls between these two series. In order to evaluate the effect of uncertainty in the observed instrumental record on the reconstructed streamflow, we expand on traditional reconstruction methods which have solely focused on error in the reconstruction model. Using the inflow and outflow records as the range of uncertainty, a Monte Carlo procedure is used to estimate error which may be distributed in the instrumental record. This information is used to create a large number of potential or hypothetical "true" natural instrumental flow series for the Klamath River. Independently calibrated tree-ring reconstructions are then generated for each of these hypothetical natural streamflow series. We are currently extending the work to turn the reconstruction probability distributions into confidence intervals and exceedance/non-exceedance probabilities to better compare past and present drought events. A final reconstruction, with confidence intervals, will be generated and compared to the reconstruction described above, and incorporated into regional analyses. These results will be published in a peer-reviewed paper.

2.4 Reconstruction – Sacramento/San Joaquin Basins

Water-year total flows were reconstructed for 10 full natural flow (FNF) series in the Sacramento and San Joaquin River basins (Table 3). All flow data were downloaded from the California Data Exchange Center of the California Department of Water Resources (http://cdec.water.ca.gov/queryTools.html). Water year totals were downloaded for the two summary series -- Sacramento River Runoff and San Joaquin River Runoff. The first is defined as the sum of Sacramento River at Bend Bridge, Feather River inflow to Lake Oroville, Yuba River at Smartville, and American River inflow to Folsom Lake. The second is defined as the sum of Stanislaus River inflow to New Melones Lake, Tuolumne River inflow to New Don Pedro Reservoir, Merced River inflow to Lake McClure, and San Joaquin River inflow to Millerton Lake. Monthly flows in acre-feet were downloaded and summed in water-year totals for the other eight gages listed in Table 3.

Tree-ring data for the reconstructions were developed by us from our own collections, as described previously, downloaded from the ITRDB, or pulled from data files at the Laboratory of Tree-Ring Research (LTRR). For ITRDB chronologies, the following screening steps were taken: 1) chronologies from California, Oregon and western Nevada in the latitude range of the target watersheds and completely covering the interval 1600-1996 CE were downloaded; 2) log-transformed flow at each of the 10 gages (Table 3) was regressed against each chronology, lagged -1, 0, and +1 years relative to the water year; and 3) a chronology was accepted into the network of candidate sites only if accounted for at least 20% of the variance of water-year flow in the regression model for at least one of the gages. The requirement that the chronology cover the period 1600-1996 CE was relaxed for blue oak (*Quercus douglasii*) sites in the ITRDB, as those are known to have an exceptionally strong moisture signal (e.g., Meko et al. 2001, 2011). Shorter chronologies from other species were deemed unlikely to improve on reconstruction accuracy available from blue oak alone over the past 300 years. Measured ring widths only (no site chronology) were available for some sites in the ITRDB. For those sites, we downloaded the ring widths and generated a site chronology using program ARSTAN to enable us to include the site in the screening exercise.

For ITRDB chronologies passing the screening, the ring widths were downloaded and subjected to additional statistical and graphical quality control using Fortran program COFECHA (Holmes 1983), and Matlab program Lockdown (unpublished, D. Meko). Individual core ring-width series were truncated or deleted as needed to eliminate problems due to questionable dating or measurement, and to reduce temporal changes in sample size in chronologies whose common signal is adequately represented by some reduced set of long ring-width series. The quality-control steps included favoring ring-width series that cover parts of the tree-ring record with low sample replication (e.g., early centuries), have long segment length (number of years), and a strong correlation with other series at the site.

The complete tree-ring network for flow reconstruction in the Sacramento and San Joaquin basins is comprised of the 61 site chronologies at sites shown on the map in Figure 2. Tables with site information and chronology statistics are included in Appendix C. All except one chronology in this network were developed by us from the measured ring widths using the standardization procedure described previously under Chronology Development. The exception, the Kern Composite site chronology of *Pinus Balfouriana* (foxtail pine), was contributed to our study by Dr. Tony Caprio, Fire Ecologist with Sequoia/Kings Canyon National Park. That chronology had been computed by Dr. Caprio using program ARSTAN and conventional detrending choices of negative exponential or straight-line fitted trends (personal communication, Tony Caprio).

Water-year-total flows at each of the 10 target gages (Table 3) in the Sacramento and San Joaquin River basins were reconstructed by locally weighted regression, or Loess (Cleveland 1979; Martinez and Martinez 2002) from subsets of site chronologies in the 61-site network. A Loess reconstruction as we define it is an interpolation of estimated flow from a smoothed scatterplot of observed flow on a single summary tree-ring variable. We used as the predictor, or tree-ring variable, an average over sites of standard chronologies that have first been filtered and scaled to accentuate their statistical signal for the target flow gage. A nested-modeling approach similar to that described by Meko (1997) and applied in reconstruction of Colorado River flow by Meko et al. (2007) was used for reconstructions. The reconstruction method was adapted specifically for this study after exploration of various alternatives, and is described in detail in Appendix D.

The reconstruction method includes cross-validation and split-sample validation to guard against over-fitting and temporal instability of models. Uncertainty in Loess-generated reconstructed values is estimated by the method of "upper and lower smooths" (Martinez and Martinez 2002), which yields an approximate 50% confidence interval around the reconstructed flows. This confidence interval is estimated by Loess modeling separately applied to scatterplots of the positive and negative reconstruction residuals against fitted values (Appendix D).

Summary statistics of reconstruction models for the 10 target gages in the Sacramento and San Joaquin basins are listed in the bottom half of Table 2. The percentage of flow variance accounted for by the "median-accuracy" model ranges from 68% for the Sacramento River (Sacramento River above Bend Bridge) to 78% for the San Joaquin River. Because these reconstructions are done with time-nested models, accuracy varies over time depending on the quality of the available tree-ring chronologies. This feature of the nested models is illustrated for the SJQ4 reconstruction in Figure 3. At the top are time plots of the annual reconstruction, unsmoothed and smoothed by a 30-yr Gaussian filter, 900-2012 CE. At the bottom are time plots of the number of chronologies, N, in the nested models and the percentage of variance, EV, accounted for by the models. Each jog in the time plots of EV and N corresponds to a change in the available set of chronologies and in the nested model. At the start of this tree-ring record, 900 CE, the network consists of just 2 chronologies and the model explains 58% of the flow variance. By the 1700s the number of chronologies in the model has risen to 16 and the EV statistic to 82%. Toward the most recent part of the record, chronologies drop out, and accuracy of reconstruction declines. EV remains at 69% through 2011, but drops sharply in 2012 because of loss of the blue oak chronology at Mt. Diablo from our network.

The high EV for these models indicate strong tracking of observed flows by reconstructions, and this quality is illustrated in the time plot of observed and reconstructed flows, 1901-2011, for San Joaquin River Runoff, or SJQ4 (Figure 4).

A defining characteristic of this system of rivers is the high inter-series correlation of annual flows. Correlation matrices for both the observed and reconstructed flows for the common period 1906-2011 underscore this strong spatial coherence in runoff (Table 4). A comparison of inter-series correlations for the observed and reconstructed flows also shows that the reconstructions slightly overstate the coherence. For example, the correlation between SAC4 and SJQ4 is 0.90 for the observed flows and 0.95 for the reconstructed flows. This is to be expected because reconstruction models for different rivers include some of the same tree-ring chronologies as predictors. The bias in inter-series correlation appears highest for widely separate basins. For example, correlation between the Merced River (MRC) and Sacramento River above Bend Bridge (SBB) is 0.79 for the observed flows and 0.94 for the reconstructions.

2.5 Analysis of Reconstructions

Methods described below address the five main analysis components of the study: (1) Place instrumental-period flow statistics in long-term context, (2) Quantify droughts and wet periods, (3) Identify cycles in wetness and dryness, (4) Check consistency of reconstructions with other paleoclimatic data, and (5) Assess reconstructed flow variations in the context of expected scenarios of climate change.

We address the following statistics of flow in a long-term context: mean, median, variance, skew, and lag-1 autocorrelation coefficient. Statistics of the long-term reconstruction are compared with those of the observed and reconstructed flows for the instrumental period. Selected statistics of the reconstruction are also computed in a moving time window to investigate the long-term variability of the statistics for over numerous available periods the same length as the instrumental period. Empirical cumulative distributions (cdf's) are used to assess the non-exceedance probability of the statistics for the instrumental period. Box plots are used to compare distributions of observed and reconstructed series over common periods of time.

Droughts and wet periods are summarized by two approaches. First is runs analysis, as described by Salas et al. (1980). A run is defined by a sequence of two or more years below the threshold. A measure of drought-duration is the run-length, or the number of years in the sequence.
Runs are summarized in tables listing the start-year, end-year, and run-length. For these tabular summaries we use the median of the time series for the analysis period as the threshold flow. Time series plots of annual reconstructed flows with runs longer than three years color-shaded are used to graphically display the time sequence of runs. The second approach used to summarize droughts and wet periods is running-means analysis. Running means of reconstructed flows are computed and ranked, and the 20 lowest running means of various length are listed in tables. Comparisons are made among the three major flow series. The temporal evolution of droughts and wet periods in terms of running means is shown graphically with color maps, or "flame plots" (Meko et al. 2011; Malevich et al. 2013). The plots, as used here, color code every combination of ending year and *m*-year period, $5 \le m \le 50 yr$, by size of anomaly in flow as a percentage of long-term mean observed flow.

Cycles in the reconstructions are summarized by spectral analysis, cross-spectral analysis, and wavelet analysis. We use the term "cycles" loosely here to include variations that are rhythmic in some sense, but do not necessarily have a regular wavelength or period, and may be present in some parts of the time series and not in others. An example might be droughts that tend to recur at 20-year intervals. Sometimes the interval may be longer or shorter than 20 years, and the intensity – as magnitude of flow anomaly – may be larger or smaller. And the fluctuation may be absent for long segments of the record. Such a "cyclic" pattern can be contrasted with a pure sine wave, which maintains the same period and amplitude at all points in time. Spectral analysis summarizes cycles by displaying the variance of the time series as a function of frequency, or its inverse – wavelength. The variance of a time series can be mathematically split up into contributions from different wavelengths. For the example just mentioned, variance would be high near wavelength 20 years. The plot of the relative variance contributed as a

function of wavelength or frequency is the spectrum. Spectral analysis allows some assessment of whether a cyclic component in the data is unexpectedly high (as from some cyclic influence on climate), as opposed to something that may reasonably be expected due to random variability. Cross-spectral analysis extends spectral analysis to multiple time series, and addresses whether cyclic variations in one flow series are related in some sense temporally with those in another flow series. The variations in two series may be in-phase (peaks occurring simultaneously, troughs occurring simultaneously), or out-of-phase (e.g., some time lag between peaks in the two series), or unrelated. In this report, we use spectral analysis to summarize cycles in individual flow series and cross-spectral analysis to summarize relationships between pairs of flow series for different rivers. Spectra and cross-spectra applied in this report use the smoothed-periodogram method (Bloomfield (2000). Preliminary steps include the following: 1) subtract the mean, 2) taper the series (5% of each end), and 3) pad the series with zeroes to such that its length is a power of two. The discrete Fourier Transforms, raw periodograms and cross-periodogram are then computed and smoothed with convoluted spans of Daniell filters to achieve spectral and cross-spectral estimates with the desired bandwidth. The mathematical and statistical operations in these methods are described in Bloomfield (2000).

Wavelet analysis (Torrence and Compo, 1998) is used in this report to investigate the temporal evolution of wavelike and possibly cyclic features in the flow series. Wavelet analysis is particularly useful for investigating wavelike features that may localized to parts of a long times series. For example, wavelet analysis can directly address whether some multi-decadal rhythm in wet and dry periods occurs in a long reconstructed streamflow series, and can identify when that rhythm is absent or present, and when the rhythm is weaker or stronger. Time-variation in the relationship between cyclic features in pairs of series is summarized with wavelet cross-coherency (Grinsted et al., 2004). For these analyses we use the Matlab-based wavelet package available for download from the National Oceanography Centre (http://noc.ac.uk/using-science/crosswavelet-wavelet-coherence). Wavelet analysis differs from spectral and cross-spectral analysis in being generally applicable to nonstationary as well as to stationary series, in not relying on the assumption that cyclic variations be sinusoidal in form, and in being specifically intended to study cyclic variations that may "come and go" over the length of the time series.

Consistency of flow reconstructions with other paleoclimatic time series representative of moisture variation is summarized with correlation analysis and smoothed time series plots. Our comparative analysis focuses on a set of hydroclimatic reconstructions from the western US, including gridpoint tree-ring-derived Palmer Drought Severity Index (PDSI) in the North American Drought Atlas (Cook et al., 2009), and flow reconstructions for the Snake (Wise 2010), Yampa (Gray et al. 2011), Colorado (Meko et al. 2007), San Juan (Woodhouse et al. 2006), and Salinas (Griffin 2007) Rivers, as well as lower Colorado River basin tributaries (Salt-Verde-Tonto River (Meko and Hirschboeck 2008). We also use this analysis to show spatial patterns of drought across the western U.S.

The relative importance of reconstructed flow variations to changes expected with climate change scenarios is summarized by comparing the maximum run-lengths (see above) of reconstructed flows, observed flows, and ensemble members of projected full natural flow (FNF) or runoff. For consistency, we used the same six downscaled GCM models, run through the VIC hydrologic model, as were used by CADWR in a 2009 climate change report (Chung et al. 2009), with one run per model, and two climate change scenarios, A2 and B1. Results from projections, 1950-2099, were compared with maximum run-lengths in observed and reconstructed series (for the observed period and full reconstruction). For the Klamath, this assessment was done using a set of downscaled CMIP3 Climate and Hydrology Projections available at http://gdo-dcp.ucllnl.org/downscaled_cmip_projections/dcpInterface.html#About (USBR 2011, see also Mauer et al. 2007). Because of difference in the units for the model projections (mm of runoff) and the flow series (Acre-feet), all series for the Klamath assessment were first scaled to z-scores using common reference-period (1951-2000) means and standard deviations. A dry year was defined as an annual value below the median for the reference period, and run-length was computed as the number of consecutive years below the threshold. For gages in the Sacramento and San Joaquin Basins, the downscaled projections already in flow units (acre-feet) appropriate for the target basins were obtained from CADWR. For these records we used as the dry-year threshold for observed flows and projections

the median of the observed water-year flows for the period 1906-2012, and as the threshold for reconstructed flows the median reconstructed flow for that same 1906-2012 base period. Our procedure was to compare maximum run-length of runs in the projection scenarios with those in the 900-2012 CE reconstructions and 1906-2012 observed flows.

3. Results

Results of application of the methods described in the previous section to the main flow reconstructions for the three basins -- the Klamath at Keno (KLK), Sacramento Four Rivers index (SAC4), and San Joaquin Four Rivers index (SJQ4) are described here. Sections 3.1-3.5 individually address the five main analysis components of the study.

3.1 Instrumental-Period Flow Statistics in Long-Term Context

Statistics of reconstructed flow or precipitation can be used to infer whether the short snapshot of time provided by the instrumental was unusually dry or wet, stable or variable, etc. Statistics are listed in Table 5 for all 16 records reconstructed in this study. Three rows of statistics are shown for each gage. The first two rows for a particular gage allow comparison of statistics of observed and reconstructed series for their common period. This comparison is useful as a baseline to check whether the reconstruction might be biased high or low for a statistic. Some bias is expected, depending on statistic. For example, the standard deviation will generally be lower in a reconstruction than in the observations for the same period because not all variance of flow or precipitation can be explained by regression. On the other hand, when ordinary least squares is used for reconstruction, the means of observed and reconstructed series are forced to be identical over the period used to calibrate the model. This explains, for example, the identical means (1176 kaf) in observed and reconstructed flow for the common period 1949-2000 for the Klamath at Keno. The median is not constrained to be equal for regression, and for the Klamath the median is biased high by 17 kaf (1142 vs 1125 kaf) in reconstruction. The skew is especially prone to negative bias in tree-ring reconstructions of flow or precipitation in semi-arid regions, where observed flow and precipitation are typically highly positively skewed in comparison to the more normally distributed tree-ring data. For example, negative bias in skew is evident for all except the Klamath at Keno reconstruction in Table 5. Lag-1 autocorrelation may or may not be biased in a tree-ring reconstruction depending on the data processing (standard vs residual chronologies) and reconstruction procedure (e.g., use of lagged predictors in models). Autocorrelation is small for all gages studied here except the Klamath at Keno, and for that record the reconstruction closely mirrors the observed autocorrelation (as was the intention in the reconstruction model development).

Reconstruction bias in skew and median, as well as the typical compression of variance by the reconstruction process are evident in box plots of selected reconstructions for the Klamath Basin (Figure 5) and Sacramento/San Joaquin basins (Figure 6).

Because statistics of tree-ring reconstructions are typically biased one way or another relative to those of the observed time series, placement of the hydrologic statistics of the short instrumental period in a long-term context is best restricted to comparisons of reconstructed data. For the statistics listed in Table 5, this comparison would be of the last two rows for a particular gage. Such a comparison allows us to address questions such as whether the modern period has been especially dry or variable in the context of the past few centuries. Restricting the comparison to reconstructed series for this assessment circumvents the problem of reconstruction bias in the statistic. For example, the 1949-2000 instrumental period for the Klamath is inferred wet in a long-term context according to both the mean (1176 vs 1104 kaf) and median (1142 vs 1113 kaf).

This comparison for the Klamath does not address the question of whether some past periods of similar length to the instrumental period were wetter or drier than the instrumental period. A more apt comparison for that objective is of the reconstruction statistic for the *m*-year instrumental period with the large sample of the corresponding statistic for all possible *m*-year periods in the long-term reconstruction.

The empirical cumulative distribution functions (cdfs) for such an assessment of variability of *m*-year mean, median, standard deviation and lag-1 autocorrelation for flow in the three main basins (Klamath at Keno, Sacramento Four Rivers and San Joaquin Four Rivers) in Figures 7-9.

These cdfs, with vertical lines plotted at the value of the statistic for the observed and reconstructed for the instrumental period, highlight especially the large variability of recent flows. For example, on the Klamath, the standard deviation of reconstructed flows for the 52-year period (1949-2000) of overlap of observed and reconstructed flows ranks at about the 75th percentile of the standard deviations for 446 different unique overlapping 52 year periods in the 1507-2003 reconstruction. Recent variability is highlighted even more strongly on the Sacramento and San Joaquin, where the standard deviation for the instrumental period ranks above the 95th percentile in a sample of more than 1000 sample standard deviations computed for 106-year (Sacramento) or 112-year (San Joaquin) periods of the reconstructions.

Whether the instrumental period is judged relatively wet or dry in a long-term context can sometimes hinge on choice of statistic to describe central tendency. For the San Joaquin (Figure 9), for example, the cdf for the mean (upper left) suggests the instrumental period was relatively wet (80th percentile of sample means), while the cdf for the median suggests the instrumental period was relatively dry (40th percentile of sample medians). Such differences can result from variable skew in the annual reconstructed flows for the different time samples. In particular, with positive skew, perhaps due to a few years of very high flow, the mean will be shifted high relative to the median. While the "typical" San Joaquin flow – that exceeded in half the years – may have been relatively low over 1901-2011, a few years with very high flow in that period could result in an arithmetic average, or mean, flow exceeding that of most prior 112-year periods.

3.2 Droughts and Wet Periods

The reconstructed flows in the Klamath, Sacramento, and San Joaquin basins allow an assessment of the instrumental period of record, in terms of drought duration and severity, in a long-term context, The longest run of below median flow years extends to 21 consecutive years in the Klamath River reconstruction, 10 years in the Sacramento and 13 years in the San Joaquin (Figure 10-12, Table 6). Two intervals of 10 years are indicated in the Sacramento: late 1200s and in the 1920s-1930s. In the San Joaquin, the 13-yr run occurs in the late 1400s. The 21-yr run in the Klamath occurs in the mid- to late 1600s. Numerous periods of low flows of four years and more are evident in all three series.

The lowest 20 single-year, 3-, 6-, 10-, 20-, and 50-yr periods are listed in Tables 7, 8, and 9. In both the Sacramento and San Joaquin, flows in the 1920s and 1930s rank among the most extreme in the context of the last millennium, as single years and multi-year periods, as well as multi-decadal periods (e.g., 20 years) of drought. Other 20th century low flows that rank in the lowest 20, are 1977 as a single and as a multi-year drought (1975-77) in both basins, and the 6-year period ending in 1992, which is the longest low flow period that ranks in the lowest 20 multi-year averages over the full reconstructions.

Reconstructions for the Sacramento and San Joaquin flag 1580 an exceptionally dry single year – far drier than any experienced in the instrumental period. On the Sacramento, the reconstructed flow for 1580 is only 45% of that of the reconstructed flow in 1924, the second driest year of the reconstruction (Table 7). The relative severity of low flow in 1580 is almost as great on the San Joaquin, where flow in 1580 is reconstructed at 54% of the flow in 1924 (Table 8). The single-year intensity of tree-ring reconstructed drought in 1580 has been noted previously (Meko et al. 2001). Our results suggest that the drought beginning in the 1570s and including 1580 was of shorter duration in the San Joaquin Basin than in the Sacramento Basin. The 1470s are also a key period of low flow in both basins. At decadal and longer time scales, pre-20th century low flow extremes are dominated by periods in the mid- to late-1100s in the Sacramento basin, while the second half of the 15th century appears to have been more severe in the San Joaquin basin (however, prolonged drought is evident for both of these periods in both basins).

The Klamath at Keno flow reconstruction, starting in 1507, is shorter than the Sacramento and San Joaquin reconstructions, and so does not provide as long a record for instrumental period assessment.

The 1920s and 1930s on the Klamath also appear to be periods of extreme low flow (single to 20-year periods), but rank in the middle to bottom of the lowest 20 periods, in contrast to the higher rankings in the Sacramento and San Joaquin records (Table 9). As in the Sacramento and San Joaquin, the early 1990s is also a period of notable drought in the Klamath basin. The years of the 1570s to early 1580s are markedly dry here as in the other two basins, but the short-term periods (single to 6-year periods) with lowest flows occur in the 1650s and 1660s (Table 9). The decadal and multidecadal periods with lowest flows in the Klamath basin are in the latter half of the 17th century. These are also periods of drought in the Sacramento and San Joaquin basin, but are less severe in those basins in the context of the last 1000 years. If we consider the long Klamath Falls precipitation reconstruction (extends to AD 1000, Malevich et al. 2013), the severe low flow periods of the 1100s in the Sacramento and San Joaquin are evident in this basin as well, although the 17th century periods of low flow are still prominent when assessed in the 1000-year context. The second half of the 11th century also appears to be exceptionally dry in the Klamath Basin (Malevich et al. 2013); this interval is dry in the Sacramento and San Joaquin, but less so than in the Klamath (e.g., Figures 11 and 12).

Flame plots, as described in the Data and Methods, can be used for a quick graphical assessment of the history of dryness and wetness in terms of moving averages of variable length. Moving averages of reconstructed flow for the Sacramento, San Joaquin and Klamath Rivers for window sizes, or moving averages, of *m* years, $5 \le m \le 50$, are graphically summarized by flame plots in Figures 13-15. These plots color-code the moving averages over the full length of the reconstructions as a percentage of normal. For the summary, we define "normal" as the long-term mean of observed flows. The dominant running-mean droughts listed in Tables 7-9 and discussed previously emerge vividly as red colors on the flame plots. At any point on a flame plot, the color indicates the percentage of normal flow for the *m*-year period ending in a given year. Window size increases along the y axis, such that short-duration, intense droughts give dark red colors restricted to the lower part of the plot, while long-duration drought or recurrent dry years over a long period give red colors toward the top of the plot. Colors, from dark red to dark blue, correspond to flow anomalies from 70% to 120% of normal, or from very dry to very wet. Any flow anomalies that happen to be more extreme than those limits are coded with the colors for 70% or 120%. As obvious in Figures 13-15, colors generally become lighter toward the top of the plot because the largest anomalies in terms of extremely high or low percentage of normal are generally found in single years or short moving averages (*m* closest to 5 yr).

Interpretation of the flame plots is illustrated by arrows A, B and C: on the plot for the Sacramento (Figure 13). Arrow A points to the mid-1100s, where red colors indicate 25-year moving averages less than 85% of normal flow. A mid-1100s drought is also a singular persistent event in a tree-ring study of the Colorado River (Meko et al. 2007), and has been flagged as an exceptional case of simultaneously dry conditions on the Sacramento and Colorado Rivers (Meko et al. 2012). The flame plot in Figure 13 indicates that the unusual severity of this drought on the Sacramento extends out to at least an averaging period of 50 years (top of plot). Arrow B points to an extended period of wetness in the 1300s. The dark blue coloring indicates 50-year moving averages of at least 120% of normal at that time. Arrow C points to the intense decadal-scale drought of the 1930s, where the dark red coloring indicates 10-year running means of less than 75% of normal flow. Sacramento River dry periods of ten to 20 years in length during a short interval in the early 20th century were the most severe (i.e. reddest) such periods in the entire record. Comparison of the 1930s drought with the mid-1100s drought on the flame plot in Figure 13 underscores the difference in drought characteristics: less severe short-term flow anomalies but longer duration of low flows in the 1100s than in the 1930s.

Comparison of flame plots in (Figures 13 vs 14) shows that the San Joaquin and Sacramento Basins share many of the major droughts and wet periods. Some differences, however, are evident in relative severity of droughts and wet periods. The 1930s drought appears in both basins, but is more severe in a long-term context in the Sacramento than in the San Joaquin. Both basins have dry conditions in the 1100s, but less so in the San Joaquin. Dry periods on the order of 30-40 years near the end of the 15th century were most severe periods of this length in the San Joaquin record (Figure 14).

In the Klamath River reconstruction, the mid-17th century stands out as a period of severe low flow conditions, from very short time periods to multi-decadal periods, while the late 16th century and the 1930s are notable for drought at periods of less than ten years (Figure 15). The Klamath also exhibits an interesting 18th century recurrence pattern of drought in which a series of short term droughts, marked by low 5-year running means, are interspersed with more normal conditions. As the averaging period is lengthened, those more severe short droughts merge to give running means of less than 90% of normal flow for averaging periods as long as 50 years ending in the latter part of the 1700s (Figure 15, top of plot).

In summary, major periods of extreme low flow are shared among the three basins, although the degree of severity varies. The 1920s and 1930s (up to 20-year periods), 1570 to the early 1580s (mostly at intervals of ten years or less) and the 1100s (prominent at 20- to 50-year intervals) are the most markedly widespread and severe periods of low flow shared across all three basins.

3.3 Cycles in Wetness and Dryness

The spectrum of a time series is the distribution of variance of the series as a function of frequency, or wavelength. A flow series with large-amplitude swings from high flows to low flows over periods of centuries has high variance at centennial timescales, or long wavelengths. A flow series that fluctuates rapidly from dry conditions to wet conditions every other year or several years has high variance at interannual timecales, or high frequencies. Spectral analysis can be used as a descriptive tool to succinctly summarize at which wavelengths or ranges of wavelength the variance of a time series is concentrated. The spectrum of a flow series with a strong, regular cycle at some wavelength (say, 20 years), will show a significant spectral peak at the wavelength of 20 years. The spectrum will show the peak, and spectral analysis will allow testing of the hypothesis that the peak results from random variability as opposed to some internal cyclic feature of the system (e.g., climate) generating the time series. We apply spectral analysis in this study to investigate possible cyclic behavior or rhythms in reconstructed and observed flow series.

The spectra of the observed and reconstructed flows for the Klamath, Sacramento and San Joaquin Rivers computed for the instrumental period are plotted Figures 16-18. These plots represent the relative variance (y axis) of the series as a function of frequency (x axis). The frequency axis ranges from 0 to 0.5 cycles/year. Wavelength is the inverse of frequency, such that a frequency of 0.1 cycles per year corresponds to a wavelength of 10 years. The x axis of the spectrum therefore covers wavelengths from infinity (left end of x axis) to 2 years (right end of x axis). The height of the plotted spectrum is proportional to the variance contributed by a range of wavelengths centered on any given point on the x axis. The spectra plotted in Figures 16-18 indicate several important points about the reconstructed and observed flows. First, the similarity in shapes of spectra for observed and reconstructed flow shows the ability of the tree-ring data to capture the variability of flow at different wavelengths. Second, the major peak in the spectrum (arrow A on Figure 16) indicates that variance in the time series is relatively high at a band of frequencies centered on frequency f=0.0625 cycles/year, or wavelength 16 years (wavelength is inverse of frequency. The location of the highest spectral peak ranges between about 14 years and 16 years for the three flow series (Figures 16-18), and is similar for the reconstructed and observed flows. Third, the spectrum for the reconstructed flows is lower than that for the observed flows. This feature merely reflects the fact that the total variance of reconstructed flow is less than that of observed flow, and is expected because tree-ring data cannot explain all of the variance in observed flow. Fourth, from the shapes of the spectra, it is apparent that the Klamath has proportionally more of its variance at the lower frequencies (longer wavelengths) than the Sacramento or San Joaquin. Spectra for the three basins are broadly similar in shape, with low-frequency variance becoming increasingly important toward the north, as indicated by the shapes of the fitted red-noise spectra (dashed lines).

Ability of the reconstructions to accurately track observed flow variations at various wavelengths or frequencies can be checked further with low-pass smoothing and cross-spectral analysis. Figures 19-

21 show a series of plots from cross-spectral analysis of observed and reconstructed flows for the same three basins discussed above. The top plot in each figure is Gaussian-smoothed observed and reconstructed flows. The smoothed time series plots highlight the synchrony in time series variations of observed and reconstructed flow at decadal-and-longer time scales. Intervals when both smoothed series are simultaneously in their lowest decile (dry) are shaded gray in the smoothed plots. The shading underscores the low-flow conditions of the 1930s and late-1980s to early 1990s. The Klamath observed series, which does not extend back to the earlier of those two droughts, shows a downward trend from the start of record (1949) to the drought peak in the early 1990s (Figure 19).

The smoothed time plots for the observed and reconstructed flow of the Sacramento and San Joaquin Rivers fluctuate greatly from one decade to another, a signature of high inter-decadal variance (Figures 20 and 21, top plots). These fluctuations are large in a practical sense. For the Sacramento (Figure 20), the fluctuations range from about 60% of normal for lowest troughs to 140% of normal for highest peaks. Peaks in wetness are found at 1915, 1941, 1952, 1970, 1983 and 1997. The intervals between peaks are annotated on the plots for the Sacramento (top, Figure 20). The average interval between peaks is 16.4 years. These time series features reflect the near-15-year spectral peak previously noted in the spectral analysis of observed and reconstructed flows for the instrumental period (Figure 17).

The two lower left plots in Figures19-21 show sample spectra of observed and reconstructed series, similar to the spectra plotted in Figures 16-18, but here with a confidence interval (dashed lines) that allows assessment of statistical significance of peaks. A peak is judged significant if the confidence interval around the spectrum at that frequency does not include the horizontal line, which represents the theoretical spectrum of white noise. White noise is a time series with the same variance as the time series analyzed, but with variance distributed evenly over all frequencies. No peak in any of the spectra in Figures 19-21 emerges as statistically significant from white noise. According, we conclude that the observed flows on the Klamath, Sacramento, and San Joaquin do not have statistically significant cycles at any particular frequency or wavelength.

The two lower right plots in Figures 19-21 are the coherency and phase spectra. The coherency is analogous to a correlation coefficient between time series as a function of frequency. The coherency plots here suggest strong correlation of observed and reconstructed series across the full range of frequencies. Coherence is especially high at frequencies for which the variance is high in the individual time series. The phase plot indicates whether the peaks and troughs in reconstructed and observed flows are times such that peaks line up with peaks and troughs with troughs (in-phase). Phase is important in a cross-spectral analysis because it is possible for coherence to be high and two series to be completely in opposition (one indicating wet when the other dry). The phase plots confirm that reconstructed flows are in-phase with observed flows at high and low frequencies in the three basins analyzed. This is especially true for frequencies at which variance is high in the individual series. In summary, the spectral and cross-spectral analysis presented so far support the idea that the tree-ring reconstructions in the three basins can be used to infer variations in observed flow at a low and high frequencies.

The cross-spectral analysis just described confirms that that the reconstructions can effectively track fluctuations in observed flow at high and low frequencies. The full-length reconstructions can therefore be applied to investigate long-term evidence for cycles in wetness and dryness. Although spectral peaks in the flow series (reconstructed and observed) for the instrumental period were found to be not significant, features not significant in a short time series may be significant in a longer time series because, other thing being equal, the width of confidence intervals for statistical tests narrow as sample size increases. The reconstructions generated here extend back to 1507 CE for the Klamath and to 900 CE for the Sacramento and San Joaquin basins. Spectra for the full-length reconstructions for the Klamath, Sacramento and San Joaquin basins are shown in Figures 22-24. These spectra are plotted along with a red noise null continuum and 95% confidence interval to facilitate identification of “significant” peaks – in this case, a peak higher than expected by chance if the series were merely red noise. Small differences in wavelength of peaks should not be interpreted, as the spectral peak is associated with a range of frequencies delineated by the bandwidth annotated on the plots. The spectrum for the full-length Klamath reconstruction shows a small spectral bump near 15 years, but the main peak, and the only peak

significantly distinguishable from a red noise spectrum is at the much longer wavelength of 57 years (Figure 22).

Spectra of the full-length Sacramento and San Joaquin reconstructions (Figures 23-24) are much less red (less dominated by low-frequencies) than that of the Klamath. This difference may reflect the greater importance of groundwater to flow of the Klamath, but it should be kept in mind that the time period of analysis for the Klamath differs from that for the other two rivers. For the Sacramento, the major peak – and the only peak statistically distinguishable from red noise – is at 102 years. The second highest peak is at 21 years. No peak in the long-term spectrum is evident at 15 years. The major peak for the San Joaquin is at just a slightly shorter wavelength (93 yr) than that for the Sacramento. Like the peak on the Sacramento, this low-frequency peak is estimated to differ significantly from a red-noise spectrum. The San Joaquin has a secondary spectral peak, which also reaches significance, at 3.7 years. This feature may represent influence of ENSO. The third largest spectral peak for the San Joaquin is at a wavelength of 21 years. The long-term reconstructions for the Sacramento and San Joaquin are alike, therefore in having their two lowest-frequency spectral peaks near 100 years and 21 years.

As described in Section 2.5, wavelet analysis is an alternative to spectral analysis as a way of studying wavelike or cyclic features in a time series, and is especially useful for studying the temporal evolution of any such features. The cross wavelet transform (XWT) and wavelet coherence (WTC) are used in combination with the continuous wavelet transform (CWT) here to graphically summarize the evolution of cyclic features in a pair of observed and reconstructed flow series. We choose for this analysis the most widely separated basins for which we have reconstructions back to 900 CE: the Sacramento River above Bend Bridge (SBB) and the San Joaquin River inflow to Millerton Reservoir (SJF). Analysis for the observed flows, 1906-2012 CE, is summarized in Figures 25-27. Analysis for the reconstructions, 900-2012 CE, is summarized in Figures 28-30.

The CWT, analogous to temporally evolving spectrum, for the observed flows shows a band of high variance near a wavelength of 15 years through the complete observed time series of SBB and SJF, with highest variance concentrated at most recent decades (Figure 25). The XWT shows at what frequencies and times the two series both have high variance, regardless of whether variations in one series are synchronous with those in the other. The XWT in Figure 26 further supports the individual CWTs in identifying the 15-year peak in variance, stronger toward the end of the series (arrow A). The WTC shows whether variations in the two series are coherent (red corresponding to highest coherence) and in-phase or out-of-phase (arrows to right, perfectly in phase; arrows to the left 180° out of phase). The red coloring and right-leaning arrows throughout the time axis near a wavelength of 15 years for the WTC in Figure 27 indicate that variations near the 15-year period in observed flow records for SBB and SJF are approximately in-phase and coherent throughout the observed record, 1906-2012.

The CWTs of the full-length, 900-2012 CE, reconstructions for SBB and SJF suggest that any cyclic tendency near a wavelength of 15 years in the individual observed flow records, 1906-2012, is a transient phenomenon, expressed best in the 20th and 21st centuries (arrow A, Figure 28). The 15-year cycle is completely absent from the first half of the SBB reconstruction (arrow B). Another interesting feature in these CWTs is the high variance near the 100-year wavelength (arrow C, figure 28). For the SBB reconstruction, this long-wave feature is present in the first half of the record, and then re-appears after 1800 CE (arrow D). For the SJF reconstruction, the feature is significant only in about the first quarter of the record. Wavelet analysis complements the spectral analysis results for the Sacramento and San Joaquin basins (Figures 23 and 24) in suggesting that the significant spectral peaks near 100 years in the full reconstruction for the Sacramento and San Joaquin are driven primarily by variations early in the reconstruction record. Some hint of this near-centennial wave is evident in the time series plots of the annual reconstructed flows for SAC4 and SJQ4. For example, the plot for SAC4 shows broad wave-like fluctuations between 900 and 1200 CE, with highs near 900, 1000, 1100 and 1200, and lows approximately midway between those highs (Figure 11).

The cross wavelet functions XWT and WTC reinforce the conclusions above on the 15-year cycle. The strongest evidence for significantly high, in-phase, common variance in SBB and SJF near 15 years is restricted to the most recent 100 years (arrow A, Figure 29). Consistently strong in-phase

coherence between the two series near wavelength 15 years is restricted to the second half of the record (arrow A, Figure 30). The XWT and XTC are consistent with the spectral analysis results discussed previously in showing a shift from around 15 years to perhaps nearer 20 years wavelength of relatively high variance before the instrumental period (red pockets centered near 1400 CE and 1800 CE at wavelengths between 16 and 32 years. In summary, this wavelet and cross wavelet analysis suggests that any observed tendency for cycles or quasi-cycles in flow records near a wavelength of 15 years in the instrumental record is not a long-term feature of the hydroclimate of the Sacramento and San Joaquin basins. The analysis also shows that cyclic behavior at very long wavelengths (near 100 years) occurs early (900-1200 CE) in the tree ring record for the Sacramento and San Joaquin Basins, but is not a regular feature over the full record.

3.4 Consistency of Reconstructions with other Paleoclimatic Data

We analyzed the consistency among the Klamath, Sacramento, and San Joaquin reconstructions with others hydroclimatic reconstructions across the western US using a set of existing reconstructions. The reconstructions for the Klamath, Sacramento, and San Joaquin Rivers were augmented with the Trinity River reconstruction to form a transect of gage reconstructions from roughly north to south across the study area. The reconstruction of Klamath Falls precipitation was also included as there is some uncertainty regarding the estimates of natural flow that were available for the reconstruction model calibration. For our assessment with other western US records, we selected a transect of flow reconstructions in the interior West, from north to south: the Snake River, the upper Colorado river basin, (the Yampa, Colorado at Lees Ferry, and San Juan Rivers), and the lower Colorado River basin (Salt and Verde Rivers with Tonto Creek flows to represent the lower Colorado River basin tributaries). We augmented the study area transect with a reconstruction of the Salinas River and several grid point reconstructions of the Palmer Drought Severity Index: 1) central Washington, 2) northeastern Nevada, and 3) southern California (called here the "west coast transect"). We also use this network to examine spatial relationships between the Klamath, Sacramento, and San Joaquin reconstructions and others hydroclimatic reconstructions.

Within the study area, the Sacramento, San Joaquin and Trinity Rivers (observed data) are all highly correlated (Table 10). The Klamath reconstructions (precipitation and flow) are less well correlated, with each other and with the other gage records, but show higher correlations with Sacramento and Trinity Rivers and somewhat lower correlations with the San Joaquin River, as would be expected. The correlations for the reconstructions over the same period reflect a very similar pattern (Table 11).

The relationships between the observed hydroclimatic series (except for PDSI, which has reconstructed values from 1949-1977) for the western US for the years 1949-2000 are shown in Table 12a. All correlations are significant ($p < 0.05$) except between the San Juan River and the lower Colorado River basin tributaries, and the western coast transect (except the San Joaquin River). In addition the correlation between the Klamath and Salinas Rivers is not significant. A comparison of the correlations with the reconstructed time series for 1949-1997 (Table 12b) shows a similar pattern, except correlations with the entire Colorado River basin for the Klamath series are not significant. In addition, the Klamath River reconstruction appears to be unrelated to other series in the west coast transect (see comments on this below).

When the patterns of correlations are examine for the reconstructions over the full common time period, 1591-1997 (Table 13a), all series are significantly correlated except the Klamath River reconstruction, which is not correlated with Colorado River basin or the southern California PDSI grid point reconstructions. In addition, Klamath Falls precipitation is not significantly correlated with the lower Colorado River basin tributaries. The strength of the correlations is as would be expected, with higher correlations among the "west coast transect" reconstructions, and lower values between the west coast and interior west reconstructions. Interestingly, the west coast correlations are highest with the northern-most interior west reconstruction, the Snake River, compared to other interior site correlations.

Correlations by century are show in Tables 13 b, c, d, and e. The pattern that emerges suggests shared hydroclimatic variability across the most of the entire region during all 100-year periods, except between the Klamath/Trinity region and parts of the Colorado River basin. This is most marked in the 17th and 19th centuries and least marked in the 18th century. In the 20th century, only the Klamath reconstructions show a lack of correlations with the Colorado River basin. In all centuries but the 20th century, the Klamath River reconstruction shows broader lack of correlations with other records, especially in comparison with Klamath Falls precipitation. This result may be evidence of the uncertainties in the estimated natural flow data used for the reconstruction calibration. This is something we will continue to investigate.

The coherence of major periods of drought in the north to south transect from central Washington to southern California can be assessed in Figure 31. Notable periods of widespread and persistent drought occurred in the 1930s, 1580s, 1100s, and 1000s (also noted in rankings and flame plots). Other periods of drought appear to have impacted subregions of this transect. For example, drought in late 16th century is evident in from the Trinity River basin and south, while not apparent in the Klamath and central Washington hydroclimatic reconstructions. A similar pattern is suggested around 1300, although the Trinity and Klamath records do not cover this period. In contrast, droughts in the late 1400s, mid 1600s and 1840s appear to have had less impact on the southern end of this transect.

3.5 Reconstructed Flow Variations in Context of Expected Scenarios of Climate Change

A number of approaches may be taken to assess drought characteristics in observed and reconstructed flow series with those in climate change projections. In this report, we chose to assess the longest run of drought. Here, we define a drought run as a consecutive period of years with values below a given threshold. For the Sacramento River at Bend Bridge and San Joaquin River at Millerton Lake, drought years were based on the 1906-2012 medians (reconstruction runs were based on the years below the reconstruction medians; observed and modeled runs were based years on years below the observed median). For the Klamath, all series were converted to z scores using the 1951-2000 period means and standard deviations before runs analysis. Thresholds for Klamath runs are medians for the reference period 1951-2000.

Bar charts (Figure 32) show maximum runs length results for the Sacramento, San Joaquin, and Klamath River reconstructions relative to the observed record in the first three bars. In all three basins, full reconstruction period runs are longer than those of the observed period (in both reconstructed and observed series) although the maximum run for the Sacramento is only slightly longer than for the observed period. The Klamath reconstruction shows a remarkable run of 21 years below the median, exceeding greatly the longest run in the observed period (nine years). The downscaled projections for the Sacramento and Klamath basins are relatively consistent over the six models and two scenarios. Run lengths for the Sacramento projections vary between four and eight years, with none reaching the maximum run length in the instrumental data (ten years). For the Klamath, run lengths vary from five to eight years, almost matching the maximum run length in the observed period, nine years. Runs are slightly longer, on average, for the A2 runs for the Klamath; they are the same, on average, for the Sacramento A2 and B1 runs. The results for the San Joaquin are somewhat different. Maximum run lengths vary widely from five years to 21 years. The average across models within a scenario is eight years for A2 and 8.5 years for B1, longer than the maximum run in the instrumental period (six years), but shorter than the maximum reconstructed run (12 years). Although difficult to gage model performance based on such a small subset of runs, these results suggest the model projections may underestimate maximum runs of drought years in the future. Note: these run lengths are slightly different than those shown in Results section 1 (Figure Runs 2 and 3) because those were based on the entire Sacramento (SAC4) and San Joaquin (SJ4) basin flows (sum of four gages) while these are for specific gages.

4. Conclusions

- Sixteen new tree-ring reconstructions of streamflow and precipitation for use in water-resources planning and operation are provided for the Klamath Basin and Sacramento and San Joaquin Basins. These reconstructions cover centuries to a millennium, and reflect long-term hydroclimatic variability on time scales beyond the reach of instrumental records.
- Reconstructions indicate that the instrumental period – the period covered by gaged flow records -- has been extremely variable in a long-term context. On the other hand, the conclusion on relative wetness of the instrumental period differs depending on whether measured by the mean or median. The median tends to give the instrumental period a drier long-term standing than the mean. This difference perhaps reflects higher positive skewness of flows in the instrumental period.
- Analysis of droughts in the reconstructions for the three basins indicates the 1920s-30s and 1990s contained periods of drought notably severe, even in a centuries- to millennium-context. However, the instrumental period does not contain the driest multi-decadal (50-yr) periods, and in the case of Klamath and San Joaquin, it does not included the longest run of drought years. On the Sacramento and San Joaquin, the instrumental record notably does not contain the record low-flow for individual years. This record-low flow is 1580 CE in both basins, and is reconstructed with only about half the water-year total flow of the driest reconstructed year (1924) of the instrumental period.
- The flow reconstructions examined contain no strong, regular cycles over their full lengths. A significant spectral peak near 100 years was found in the Sacramento and San Joaquin reconstructions. That peak appears to be driven mainly by fluctuations before 1200 CE, with a hint of recurrence in the last century.
- Cyclic variation, with an average wavelength of about 15 years, is evident in both observed and reconstructed flow series over the past 100 years, but is not a long-term feature of the hydroclimate of the basins studied. While some observed flow records have large inter-decadal swings, the near-15-year cycle in those records does not pass spectral analysis tests for statistical significance.
- Comparison of observed and reconstructed hydroclimatic series in the Klamath, Sacramento, and San Joaquin basins suggests the reconstructions reflect the spatial relationships in the observed record. When a set of westerns US hydroclimatic records is considered, our reconstructions appear to replicate the spatial relationships in the observed records over the instrumental period. The major exception is the Klamath at Keno reconstruction (also notable over full reconstruction common time period), suggesting a possible problem with this reconstruction.
- Although this is a limited assessment, an evaluation of drought run length in six downscaled GCM flow projections with flow reconstructions suggests that GCMs many projections may not reflect the run lengths that have occurred under natural variability.

5. Acknowledgments

Brewster Malevich contributed to all phases of the Klamath work, which formed the framework of his masters thesis and is currently being applied toward his dissertation. Holly Faulstich, Mark Losleben and John Danloe also helped in field and laboratory work on the Klamath.

The following individuals contributed to the Sacramento/San Joaquin work: Ellis Margolis in field work and dating; Anna Penaloza in wood processing, dating and measurement; Jim Burns in dating; Mark Losleben, Alma Pemattei and Michael Zumwalt in field work; and John Carroll, Charles Golden, Rebecca Renteria and Leawna Brouduer in wood processing and measurement.

We thank Tony Caprio for generously providing *Pinus balfouriana* tree-ring data not available in the public domain, and Malcolm Hughes and Chris Baisan for helpful suggestions for field collections to update *Sequoia giganteum* chronologies. We thank contributors to the International Tree-Ring Data Bank (ITRDB) for making their chronologies freely available for studies such as ours (see Appendix C for

individual attributions). Special thanks for ITRDB data is due to Dave Stahle, Matt Therrell, Dan Griffin and their collaborators for development of the *Quercus douglasii* tree-ring network.

This work was made possible by funding from the California Department of Water Resources (CADWR). We thank Jeanine Jones of the CADWR for her encouragement and support. Downscaled GCM projections for Sacramento and San Joaquin flow were provided by Francis Chung and Jianzhong Wang of CADWR. Klamath at Keno estimated natural flows were provided by Maury Roos, CADWR. Additional funding for this project was provided by the U.S. Bureau of Reclamation Watersmart program (Agreement # R11 AP 81 457).

6. References

Akaike, H., 1974. A new look at the statistical model identification. *IEEE Transactions on Automatic Control*, 19 (6), 716–723.

Bloomfield, P. 2000. *Fourier Analysis of Time Series: An Introduction*, 2nd ed., John Wiley & Sons, New York, 261 pp.

Box, G., G. M. Jenkins, and G. Reinsel, 1994. *Time Series Analysis: Forecasting & Control*. 3rd ed., Prentice Hall.

Bunn, A. G., 2010. Statistical and visual crossdating in R using the dplR library. *Dendrochronologia*, 28, 251–258.

Chung, F., and 14 others. 2009. Using Future Climate Projections to Support Water Resource Decision Making in California. A report from California Climate Change Center, http://www.water.ca.gov/pubs/climate/using_future_climate_projections_to_support_water_resources_decision_making_in_california/usingfutureclimateprojtosuppwater_jun09_web.pdf

Cleveland, W. S., 1979. Robust locally weighted regression and smoothing scatterplots, *J. Am. Stat. Assoc.*, 74, 829–836.

Cook, E. R. and K. Peters, 1981. The smoothing spline: a new approach to standardizing forest interior tree-ring width series for dendroclimatic studies. *Tree-Ring Bulletin*, 41, 45–53.

Cook, E. R., C. A. Woodhouse, C. M. Eakin, D. M. Meko, and D. W. Stahle, 2004. Long-term aridity changes in the western United States, *Science*, 306, 1015–1018.

Cook E.R, et al. 2009. Megadroughts in North America: Placing IPCC projections of hydroclimatic change in a long-term paleoclimate context. *J. Quaternary Sci*. doi: 10,1002/jqs.1303.

Gray, S. T., J. J. Lukas, C. A. Woodhouse, 2011. Millennial-length records of streamflow from three major upper Colorado River tributaries. *Journal of the American Water Resources Association*, 47, 704-712. DOI: 10.1111/j.1752-1688.2011.00535.x

Grinsted, A., J. C. Moore, and S. Jevrejeva, 2004. Application of the cross wavelet-transform and wavelet coherence to geophysical time series, *Nonlinear Proc. Geoph.*, 11, 561–566.

Griffin, R.D,. 2007. A 600-Year Streamflow History in the Salinas Valley Reconstructed from Blue Oak Tree Rings. M.A. Thesis. University of Arkansas, Fayetteville. 67 pages.

Holmes, R., 1983. Computer assisted quality control in tree-ring standardization. *Tree-Ring*

Bulletin, 43, 69–75.

Maurer, E. P., L. Brekke, T. Pruitt, and P. B. Duffy, 2007. 'Fine-resolution climate projections enhance regional climate change impact studies', *Eos Trans. AGU*, 88, 504.

Malevich, S.B., C.A. Woodhouse, D.M. Meko, 2013. Tree-ring reconstructed hydroclimate of the Upper Klamath basin. *Journal of Hydrology*, 495, 13-22.

Martinez, W. L., and A. R. Martinez, 2002. *Computational Statistics Handbook with MATLAB*, Chapman & Hall/CRC, New York, 591 pp.

Meko, D.M., 1997., Dendroclimatic reconstruction with time varying predictor subsets of tree indices, *J. Clim*., 10, 687–696.

Meko, D. M., E. R. Cook, D. W. Stahle, C. W. Stockton, and M. K. Hughes, 1993. Spatial patterns of tree-growth anomalies in the United States and southeastern Canada, *J. Climate*, 6, 1773–1786.

Meko, D.M. and K. Hirschboeck, 2008. LTRR-SRP-II. The Current Drought In Context: A Tree-Ring Based Evaluation of Water Supply Variability for the Salt-Verde River Basin Final Report.http://fp.arizona.edu/kkh/srp2.htm

Meko, D. M., D. W. Stahle, D. Griffin, and T. A. Knight, 2011. Inferring precipitation-anomaly gradients from tree rings, *Quatern. Int*., 235, 89–100.

Meko, D. M., M. D. Therrell, C. H. Baisan, and M. K. Hughes, 2001. Sacramento River flow reconstructed to A.D. 869 from tree rings. *Journal of the American Water Resources Association*, 37, 1029–1039.

Meko, D.M., C.A Woodhouse, C.A. Baisan., T. Knight, J.J. Lukas, M.K. Hughes, and M.W. Salzer, 2007. Medieval Drought in the Upper Colorado River Basin. *Geophysical Research Letters* 34, L10705.

Meko, D. M., C. A. Woodhouse, and K. Morino, 2012. Dendrochronology and links to streamflow, *J. Hydrol*., doi: 10.1016/j.jhydrol.2010.11.041.

Michaelsen, J., 1987. Cross-validation in statistical climate forecast models. *Journal of Climate and Applied Meteorology* 26, 1589−1600.

Osborn, T. J., K. R. Briffa, and P. D. Jones (1997), Adjusting variance for sample-size in tree-ring chronologies and other regional mean timeseries, *Dendrochronologia*, 15, 89– 99.

Salas, J. D., J. W. Delleur, V. Yevjevich, and W. L. Lane, 1980. *Applied Modeling of Hydrologic Time Series*, Water Resources Publications, P.O. Box 630026, Highlands Ranch, Colorado, USA 80163-0026, 485 pp.

Stokes, M. A., and T. L. Smiley, 1996. *An Introduction to Tree-Ring Dating*, 73 pp., Univ. of Ariz. Press, Tucson. (originally published 1968, University of Chicago Press).

Torrence, C., and G. P. Compo, 1998. A practical guide to wavelet analysis, *Bull. Amer. Meteorol. So*c., 79, 61–78.

USBR, 2011. 'West-Wide Climate Risk Assessments: Bias-Corrected and Spatially Downscaled Surface Water Projections', Technical Memorandum No. 86-68210-2011-01, prepared by the U.S. Department of the Interior, Bureau of Reclamation, Technical Services Center, Denver, Colorado. 138pp.

Wigley, T. M. L., K. R. Briffa, and P. D. Jones, 1984. On the average value of correlated time series, with applications in dendroclimatology and hydrometeorology, *J. Clim. Appl. Meteorol*., 23, 201–213.

Wise, E. K., 2010. Tree ring record of streamflow and drought in the upper Snake River. *Water Resources Research*, 46, W11529, doi:10.1029/2010WR009282.

Woodhouse, C.A., S.T. Gray, and D.M. Meko, 2006. Updated streamflow reconstructions for the Upper Colorado River basin. *Water Resources Research* 42, W05415. doi:10.1029/2005WR004455.

Tables

Table 1. Field collections.

No.	Code	Site Name	Lat	Lon	Elev (ft)	Species	#Samp[a]	#Dated	#Meas	First Year	Last Year
	Klamath										
1	ALU	Antelope Lake (merged), CA	40.11	-120.64	4774	PIPO	48	45	45	1450	2010
2	BCU	Boles Creek (merged)	41.84	-120.88	4948	JUOC	49	39	34	1152	2010
3	CBY	Canby	41.50	-120.99	4892	PIPO	52	34	33	1669	2010
4	DRU	Dalton Reservoir (merged)	41.67	-120.98	5023	PIPO	48	43	41	1357	2010
5	FBK	Frederick Butte (merged)	43.59	-120.44	5249	JUOC	38	37	37	936	2010
6	HRK	Horse Ridge (merged)	43.98	-121.07	3773	JUOC	33	23	19	830	2010
7	ILM	Isn't Likely Mountain	42.12	-120.57	4898	JUOC	71	63	60	1655	2010
8	LVU	Lakeview (merged)	42.12	-120.56	4931	PIPO	52	42	39	1421	2010
9	LCU	Lemon Canyon (merged)	39.58	-120.30	5577	PIJE	48	45	46	1415	2010
10	LJK	Little Juniper Mountain (me	43.13	-119.87	5236	JUOC	38	28	23	1337	2010
11	LTU	Log Cabin (merged)	37.95	-119.15	8199	PIJE	48	41	41	1304	2010
12	PPB	Porcupine Butte	41.43	-121.61	4623	PIPO	52	41	41	1581	2010
13	SMU	Sharp Mt. (merged)	41.72	-121.82	4403	JUOC	51	41	38	1548	2010
14	AGK	Table Rock-Arrow Gap (merge	43.18	-120.90	4652	JUOC	28	28	14	530	2010
15	TMU	Timbered Mountain (merged)	41.72	-120.75	5203	JUOC	49	41	41	1654	2010
	Sacramento/San Joaquin										
16	EVG	Evans Grove	36.78	-118.82	7162	SEGI	40	40	39	1399	2011
17	KAI	Kaiser Pass	37.31	-119.11	8809	JUOC	40	38	39	1161	2011
18	LVF	Leavitt Falls	38.34	-119.55	7218	PIJE	46	42	42	1572	2011
19	UCJ	Upper Casacade Creek Junipe	38.58	-119.81	7766	JUOC	73	62	62	80	2011
20	UCP	Upper Casacade Creek Pine	38.58	-119.80	7766	PIJE	44	42	42	1556	2011
21	STA	Stanislaus River	38.41	-120.05	6657	PIJE	27	27	27	1633	2011
22	EPW	Ebbetts Pass West	38.54	-119.82	8530	JUOC	66	59	59	5	2011
23	LUP	Luther Pass Pine	38.79	-119.95	7949	PIJE	52	52	52	1463	2011
24	CPL	Carson Pass Lower	38.70	-119.99	8323	JUOC	32	31	31	1478	2011
25	SDN	Sardine Point	39.55	-120.20	7441	JUOC	55	53	53	831	2012
26	DIA	Mt Diablo	37.88	-121.97	597	QUDG	15	14	14	1853	2012
27	CSP	Calaveras State Park	38.24	-120.27	4528	SEGI	68	64	64	1522	2012
28	MHM	Mountain Home	36.24	-118.67	6463	SEGI	46	36	36	1584	2012
29	BMN	Black Mountain	36.10	-118.66	6398	SEGI	45	39	39	1516	2012

[a]Number of samples is number of cores; for sites with cross-sections from July 2013 field work, each section counted as a sample

Table 2. Reconstruction model statistics[a]

	Re[b]	RMSE[c]	adj R2[d]	R2[e]	Period[f] calibration	reconstruction
Klamath sites						
Klamath-Keno, Flow	0.65	288	0.71	0.76	1949 – 2000	1507 – 2003
Trinity, Flow	0.64	353	0.66	0.68	1912 – 2003	1584 – 2003
Klamath Falls, P						
short model	0.53	2.50	0.58	0.60	1896 – 2003	1610 – 2004
long model	0.49	2.57	0.52	0.53	1896 – 2010	1000 – 2010
Weaverville, P	0.47	7.880	0.52	0.55	1904 – 2003	1584 – 2003
Yreka, P	0.47	4.258	0.51	0.54	1872 – 2003	1531 – 2003
California sites, Flow						
Feather R.	0.68	1200	N/A	0.70	1906 – 2012	900 – 2012
Yuba R.	0.69	607	N/A	0.71	1901 – 2012	900 – 2012
American R.	0.70	780	N/A	0.72	1901 – 2012	900 – 2012
Sacramento R.	0.65	1953	N/A	0.68	1906 – 2012	900 – 2012
Sacramento 4R	0.70	4238	N/A	0.73	1906 – 2012	900 – 2012
Stanislaus R.	0.72	322	N/A	0.74	1901 – 2012	900 – 2012
Tuolumne R.	0.77	429	N/A	0.78	1901 – 2012	900 – 2012
Merced R.	0.74	276	N/A	0.75	1901 – 2012	900 – 2012
San Joaquin R.	0.76	458	N/A	0.78	1901 – 2012	900 – 2012
San Joaquin 4R	0.75	1480	N/A	0.77	1901 – 2012	900 – 2012

[a]Statistics for California sites are median values for nested models; RMSE for Klamath-Keno is before restoring autocorrelation to flow (model described in text)

[b]Reduction-of-error statistic

[c]Root Mean Square Error of cross-validation; units kaf for flow reconstructions (Flow), and inches for precipitation (P) reconstructions

[d]Adjusted R-squared statistic for Klamath sites; not available for Loess models (Calif. Sites)

[e]Regression R-squared statistic for Klamath sites; equivalent variance-explained statistic for California sites (see text)

[f]First and last year of period for calibration and reconstruction. For nested model (Calif. Sites), end year of calibration period varies between 1989 and 2012 depending on model.

Table 3. Full natural flow records[a] reconstructed in Sacramento and San Joaquin basins.

N	Code[b]	River	Period[c]	Mean(kaf)[d]
1	FTO	Feather	1906-2012	4469
2	YRS	Yuba	1901-2012	2365
3	AMF	American	1901-2012	2734
4	SBB	Sacramento	1906-2012	8443
5	SAC4	Sacramento4	1906-2011	18019
6	SNS	Stanislaus	1901-2012	1175
7	TLG	Tuolumne	1901-2012	1910
8	MRC	Merced	1901-2012	997
9	SJF	San Joaquin	1901-2012	1815
10	SJQ4	San Joaquin4	1901-2011	5926

[a]Full natural flows downloaded 06-Oct-2012 from California Data Exchange Center (cdec)

[b]Gage code in cdec (except SAC4 and SJQ4,which are summary series defined byce cdec as Sacramento River Runoff and San Joaquin River Runoff

[c]Data period (water years) for computation of mean annual flow

[d]Mean annual flow (kaf)

Table 4. Inter-series correlation[a] of observed and reconstructed flows.

	YRS	AMF	SBB	SAC4	SNS	TLG	MRC	SJF	SJQ4
FTO	0.98(0.98)	0.96(0.96)	0.94(0.98)	0.99(0.98)	0.93(0.95)	0.91(0.96)	0.88(0.95)	0.86(0.93)	0.90(0.96)
YRS		0.98(0.98)	0.89(0.97)	0.97(0.98)	0.94(0.96)	0.93(0.96)	0.89(0.94)	0.87(0.93)	0.92(0.96)
AMF			0.85(0.94)	0.95(0.96)	0.97(0.99)	0.96(0.98)	0.93(0.95)	0.90(0.94)	0.95(0.97)
SBB				0.97(0.99)	0.83(0.93)	0.82(0.95)	0.79(0.94)	0.80(0.92)	0.82(0.95)
SAC4					0.92(0.94)	0.91(0.96)	0.88(0.94)	0.87(0.92)	0.90(0.95)
SNS						0.99(0.98)	0.97(0.96)	0.95(0.96)	0.99(0.98)
TLG							0.99(0.99)	0.97(0.98)	1.00(1.00)
MRC								0.99(0.99)	1.00(0.99)
SJF									0.99(0.98)

[a]first number is for observed flow; number in parentheses is for reconstruction; all correlations for period 1906-2011

Table 5. Flow statistics for instrumental period and full reconstruction

	Time Series[a]		Period[b]	Statistic[c] Mean	Median	StDev	Skew	r_1
1	**KLK**	**Klamath at Keno Flow**	**Obs**	**1949-2000**	**1176**	**1125**	**357**	**0.05**	**0.44**
			Rec	1949-2000	1176	1142	311	-0.13	0.39
			Rec	1507-2003	1104	1113	284	-0.11	0.40
2	**TRN**	**Trinity Flow**	**Obs**	**1912-2003**	**1275**	**1129**	**589**	**0.66**	**0.09**
			Rec	1912-2003	1275	1287	487	0.18	0.23
			Rec	1584-2003	1312	1315	415	-0.18	0.17
3	**KFL**	**Klamath Falls Long P**	**Obs**	**1896-2010**	**13.33**	**13.19**	**3.61**	**0.25**	**-0.05**
			Rec	1896-2010	13.32	13.66	2.63	-0.46	-0.11
			Rec	1000-2010	13.34	13.54	2.91	-0.17	-0.08
4	**KFS**	**Klamath Falls Short P**	**Obs**	**1896-2004**	**13.42**	**13.39**	**3.66**	**0.20**	**-0.06**
			Rec	1896-2004	13.45	13.74	2.85	-0.41	-0.07
			Rec	1610-2004	13.43	13.62	2.52	-0.17	-0.04
5	**WEA**	**Weaverville P**	**Obs**	**1904-2003**	**34.66**	**33.39**	**10.91**	**0.33**	**-0.06**
			Rec	1904-2003	34.66	35.50	8.12	0.14	0.10
			Rec	1584-2003	34.82	35.75	7.43	-0.21	0.04
6	**YRK**	**Yreka P**	**Obs**	**1872-2003**	**17.72**	**17.43**	**5.89**	**0.42**	**-0.07**
			Rec	1872-2003	17.72	18.16	4.34	-0.32	0.04
			Rec	1531-2003	17.72	17.89	4.11	-0.14	0.06
7	**FTO**	**Feather Flow**	**Obs**	**1906-2012**	**4469**	**3952**	**2098**	**0.55**	**0.07**
			Rec	1906-2012	4539	4333	1755	0.15	0.18
			Rec	900-2012	4565	4364	1519	0.09	0.06
8	**YRS**	**Yuba Flow**	**Obs**	**1901-2012**	**2365**	**2252**	**1081**	**0.31**	**0.05**
			Rec	1901-2012	2427	2440	910	-0.13	0.14
			Rec	900-2012	2434	2473	801	-0.23	-0.01
9	**AMF**	**American Flow**	**Obs**	**1901-2012**	**2734**	**2588**	**1417**	**0.50**	**0.05**
			Rec	1901-2012	2786	2761	1168	0.10	0.06
			Rec	900-2012	2766	2769	1034	-0.02	-0.01
10	**SBB**	**Sacramento Flow**	**Obs**	**1906-2012**	**8443**	**7770**	**3282**	**0.63**	**0.12**
			Rec	1906-2012	8544	8235	2748	0.35	0.27
			Rec	900-2012	8576	8503	2291	0.13	0.14
11	**SAC4**	**Sacramento4 Flow**	**Obs**	**1906-2011**	**18019**	**16315**	**7686**	**0.48**	**0.09**
			Rec	1906-2011	18238	17403	6589	0.16	0.18
			Rec	900-2012	18261	17800	5602	0.04	0.07
12	**SNS**	**Stanislaus Flow**	**Obs**	**1901-2012**	**1175**	**1116**	**603**	**0.64**	**0.04**
			Rec	1901-2012	1202	1202	516	0.25	0.11
			Rec	900-2012	1181	1173	449	0.10	0.02
13	**TLG**	**Tuolumne Flow**	**Obs**	**1901-2012**	**1910**	**1878**	**903**	**0.62**	**0.03**
			Rec	1901-2012	1946	1868	789	0.35	0.13
			Rec	900-2012	1903	1857	683	0.27	0.04
14	**MRC**	**Merced Flow**	**Obs**	**1901-2012**	**997**	**919**	**538**	**0.79**	**0.03**
			Rec	1901-2012	1019	943	473	0.46	0.05
			Rec	900-2012	999	947	404	0.39	-0.02
15	**SJF**	**San Joaquin Flow**	**Obs**	**1901-2012**	**1815**	**1679**	**936**	**0.81**	**0.02**
			Rec	1901-2012	1862	1676	851	0.58	0.06
			Rec	900-2012	1798	1699	702	0.46	0.01
16	**SJQ4**	**San Joaquin4 Flow**	**Obs**	**1901-2011**	**5926**	**5610**	**2949**	**0.68**	**0.05**
			Rec	1901-2011	6016	5614	2629	0.45	0.11
			Rec	900-2012	5882	5598	2260	0.37	0.04

[a]Name of observed (Obs) or reconstructed (Rec) series, preceded by letter code used elsewhere in report to define series; all series are water-year totals of either river flow (Flow) or precipitation (p).

[b]Time period for computation of statistics; for Obs, period is overlap of available data of observations and reconstructions; for Rec, period is full length of reconstruction available beginning with year 900.

[c]Statistics: sample mean, median, standard deveiation, skew, and lag-1 autocorrelation; units for first three statistics are thousands of acre-ft (KAF) for flow, and inches for precipitation; last two statistics are dimensionless.

Table 6. Runs[a] with length ≥4 years in three flow reconstructions

Klamath[b]			Sacramento4[c]			San Joaquin4[d]	
Years	N		Years	N		Years	N
1515-1522	8		921- 924	4		946- 950	5
1540-1543	4		945- 950	6		977- 981	5
1547-1552	6		975- 981	7		1072-1075	4
1578-1582	5		1072-1075	4		1143-1148	6
1592-1597	6		1130-1136	7		1155-1158	4
1642-1646	5		1143-1148	6		1172-1177	6
1648-1668	21		1150-1158	9		1210-1213	4
1738-1744	7		1170-1177	8		1233-1239	7
1756-1761	6		1233-1239	7		1294-1301	8
1764-1767	4		1292-1301	10		1395-1402	8
1775-1779	5		1390-1393	4		1407-1410	4
1783-1787	5		1395-1400	6		1425-1428	4
1792-1798	7		1407-1410	4		1450-1461	12
1843-1846	4		1425-1432	8		1463-1466	4
1848-1852	5		1451-1457	7		1471-1483	13
1873-1876	4		1475-1483	9		1505-1508	4
1880-1884	5		1515-1521	7		1518-1523	6
1912-1915	4		1540-1543	4		1540-1545	6
1917-1920	4		1569-1572	4		1569-1572	4
1924-1935	12		1578-1582	5		1578-1582	5
1987-1992	6		1592-1595	4		1592-1595	4
			1636-1639	4		1629-1632	4
			1645-1648	4		1645-1648	4
			1652-1655	4		1652-1655	4
			1753-1760	8		1688-1691	4
			1780-1783	4		1753-1757	5
			1843-1846	4		1780-1783	4
			1856-1859	4		1793-1796	4
			1917-1922	6		1843-1846	4
			1926-1935	10		1855-1859	5
			1946-1951	6		1928-1931	4
			1959-1962	4		1946-1950	5
			1987-1992	6		1959-1962	4
						1987-1992	6
						2000-2004	5

[a]runs defined as consecutive years below median

[b]Klamath at Keno, 1507-2003; median =1113 kaf

[c]Sacramento R. Runoff, 900-2012, median=17800 kaf

[d]San Joaquin R. Runoff, 900-2012, median=5598 kaf

Table 7. Ranked moving average of reconstructed flow, Sacramento River Runoff (series SAC4), 900-2012 CE. Moving averages of length 1, 3, 6, 10, 20, 25 and 50 years ranked from driest (1) to 20th driest (20). Rank listed in first column, Flow in kaf followed by last year of moving average in remaining columns.

N	1	3	6	10	20	50
1	2399 (1580)	8747 (1580)	10864 (1934)	12341 (1933)	13691 (1936)	15601 (1175)
2	5329 (1924)	8837 (1581)	11734 (1992)	12405 (1935)	13807 (1935)	15670 (1177)
3	5339 (1729)	9228 (1796)	11778 (1933)	12661 (1934)	13867 (1937)	15682 (1179)
4	5973 (1977)	9361 (1931)	11808 (1846)	13015 (1931)	13881 (1158)	15710 (1178)
5	6071 (1829)	9832 (1655)	11905 (1931)	13079 (1932)	14304 (1934)	15768 (1176)
6	6128 (1841)	9862 (1977)	11935 (1935)	13216 (1936)	14331 (1162)	15768 (1180)
7	6161 (1783)	10023 (1778)	12225 (1480)	13552 (1580)	14338 (1157)	15834 (1174)
8	6209 (1795)	10759 (1783)	12562 (1481)	13554 (1482)	14385 (1159)	15866 (1172)
9	6231 (1931)	10875 (1845)	12600 (1932)	13561 (1937)	14459 (1939)	15940 (1173)
10	6633 (1571)	11019 (981)	12642 (1929)	13648 (1148)	14517 (1156)	15968 (1181)
11	6732 (1126)	11100 (1146)	12673 (1845)	13846 (1483)	14616 (1938)	16037 (1183)
12	6799 (1532)	11369 (1961)	12719 (1148)	13881 (1481)	14695 (1160)	16037 (1187)
13	6913 (1864)	11433 (1481)	12745 (1156)	13933 (1783)	14702 (1161)	16038 (1171)
14	6918 (1529)	11491 (1757)	12792 (1520)	13934 (1152)	14817 (1148)	16070 (1170)
15	7357 (1632)	11495 (1156)	12835 (1157)	13993 (1929)	14859 (1164)	16119 (1188)
16	7441 (1285)	11527 (1846)	12845 (981)	14055 (1849)	14874 (1152)	16148 (1168)
17	7489 (957)	11567 (1992)	12953 (1521)	14089 (1157)	14886 (1154)	16156 (1189)
18	7512 (1691)	11591 (1145)	12958 (1580)	14110 (1480)	14903 (1940)	16157 (1182)
19	7596 (1579)	11600 (1933)	12966 (1844)	14112 (1159)	14925 (1155)	16161 (1185)
20	7616 (1976)	11650 (980)	13021 (1158)	14115 (1158)	14934 (1163)	16163 (1186)

Table 8. Ranked moving average of reconstructed flow, San Joaquin River Runoff (series SJQ4), 900-2012 CE. Moving averages of length 1, 3, 6, 10, 20, 25 and 50 years ranked from driest (1) to 20th driest (20). Rank listed in first column, Flow in kaf followed by last year of moving average in remaining columns.

N	1	3	6	10	20	50
1	575 (1580)	2292 (1655)	3377 (1846)	3825 (1933)	4390 (1465)	4940 (1500)
2	1064 (1924)	2376 (1796)	3429 (1931)	3904 (1461)	4424 (1466)	4973 (1499)
3	1185 (1795)	2402 (1580)	3438 (1934)	3939 (1934)	4447 (1468)	4987 (1501)
4	1277 (1532)	2499 (1931)	3505 (983)	3941 (1459)	4466 (1469)	5016 (1483)
5	1284 (1126)	2590 (1581)	3600 (1480)	3968 (1460)	4519 (1935)	5023 (1492)
6	1453 (1729)	2663 (1778)	3668 (1845)	3971 (1935)	4522 (1936)	5026 (1480)
7	1473 (1829)	2725 (1845)	3686 (981)	3978 (1482)	4574 (1467)	5029 (1497)
8	1564 (1864)	2782 (1783)	3700 (982)	4004 (1931)	4602 (1937)	5038 (1502)
9	1593 (957)	2836 (1961)	3729 (1933)	4011 (1783)	4614 (1158)	5041 (1479)
10	1666 (1632)	2940 (980)	3732 (1783)	4019 (1932)	4632 (1464)	5042 (1481)
11	1687 (1841)	2976 (981)	3759 (980)	4056 (1483)	4634 (1463)	5048 (1498)
12	1687 (1931)	3068 (1846)	3765 (1782)	4060 (984)	4646 (1934)	5060 (1495)
13	1697 (1783)	3082 (1757)	3766 (1992)	4064 (1481)	4660 (1462)	5066 (1493)
14	1719 (1579)	3102 (1977)	3769 (1929)	4099 (1480)	4670 (1461)	5067 (1482)
15	1768 (1782)	3111 (1858)	3784 (1481)	4145 (1784)	4676 (1483)	5070 (1485)
16	1834 (1655)	3131 (1654)	3858 (1461)	4197 (1465)	4687 (1157)	5077 (1486)
17	1893 (1777)	3194 (979)	3875 (1457)	4238 (986)	4703 (1482)	5081 (1491)
18	1902 (1059)	3201 (1737)	3877 (1459)	4275 (1462)	4704 (1156)	5085 (1496)
19	1908 (954)	3205 (1824)	3887 (1670)	4275 (1849)	4717 (1159)	5097 (1487)
20	1967 (1529)	3217 (1795)	3908 (1844)	4279 (983)	4717 (1859)	5100 (1484)

Table 9. Ranked moving average of reconstructed flow, Klamath at Keno (series KLK), 1507-2003 CE. Moving averages of length 1, 3, 6, 10, 20, 25 and 50 years ranked from driest (1) to 20th driest (20). Rank listed in first column, Flow in kaf followed by last year of moving average in remaining columns.

N	1	3	6	10	20	50
1	252 (1655)	405 (1656)	492 (1660)	591 (1661)	712 (1667)	955 (1668)
2	324 (1666)	454 (1657)	504 (1659)	599 (1662)	713 (1668)	955 (1674)
3	379 (1575)	521 (1581)	579 (1661)	612 (1663)	745 (1669)	957 (1667)
4	384 (1656)	530 (1660)	583 (1658)	614 (1660)	753 (1670)	957 (1675)
5	390 (1659)	557 (1661)	591 (1657)	646 (1664)	757 (1671)	959 (1673)
6	396 (1992)	565 (1655)	638 (1656)	663 (1659)	759 (1666)	960 (1676)
7	428 (1667)	581 (1668)	653 (1662)	689 (1667)	771 (1672)	964 (1671)
8	465 (1918)	588 (1580)	684 (1582)	707 (1658)	775 (1662)	964 (1672)
9	468 (1581)	588 (1582)	692 (1934)	719 (1666)	777 (1663)	965 (1669)
10	474 (1616)	596 (1667)	696 (1663)	719 (1668)	782 (1661)	965 (1677)
11	478 (1889)	597 (1933)	697 (1580)	725 (1665)	784 (1673)	966 (1670)
12	495 (1933)	601 (1658)	712 (1581)	735 (1657)	787 (1664)	972 (1679)
13	503 (1860)	603 (1659)	734 (1583)	754 (1933)	787 (1665)	973 (1666)
14	510 (1660)	641 (1778)	735 (1664)	763 (1934)	808 (1660)	975 (1678)
15	515 (1776)	641 (1934)	740 (1655)	775 (1935)	814 (1674)	976 (1665)
16	546 (1579)	659 (1920)	743 (1933)	792 (1583)	842 (1936)	977 (1664)
17	548 (1580)	665 (1992)	744 (1935)	797 (1584)	845 (1934)	979 (1680)
18	570 (1926)	673 (1919)	754 (1667)	798 (1582)	846 (1659)	979 (1681)
19	575 (1639)	677 (1926)	781 (1936)	799 (1656)	850 (1935)	982 (1663)
20	578 (1654)	703 (1662)	782 (1668)	823 (1581)	854 (1937)	991 (1662)

Table 10. Correlations for observed flow and precipitation in the Klamath, Sacramento, and San Joaquin basins, 1949-2000. All values significant at $p < 0.05$.

	Klamath Falls P	Klamath R.	Trinity R.	Sacramento R.	San Joaquin R.
Klamath Falls P	1.000				
Klamath R.	0.752	1.000			
Trinity R.	0.719	0.674	1.000		
Sacramento R.	0.773	0.678	0.941	1.000	
San Joaquin R.	0.689	0.515	0.840	0.927	1.000

Table 11. Correlations for reconstructed flow and precipitation in the Klamath, Sacramento, and San Joaquin basins, 1949-2000. All values significant at $p < 0.05$.

	Klamath Falls P	Klamath R.	Trinity R.	Sacramento R.	San Joaquin R.
Klamath Falls P	1.000				
Klamath R.	0.671	1.000			
Trinity R.	0.699	0.724	1.000		
Sacramento R.	0.715	0.640	0.950	1.000	
San Joaquin R.	0.641	0.481	0.880	0.952	1.000

Table 12. Correlations for observed flow and precipitation in the Klamath, Sacramento, and San Joaquin basins, with other hydroclimatic series in the western US. PDSI records are reconstructions up to 1978, then are instrumental data. Common period is 1949-2000, except for Snake R. which starts in 1958. N = 48 because of four missing values in the Salinas River record. Red values are not significant at $p < 0.05$. b. Correlations for reconstructed series.

a. observed	Klamath Falls P	Klamath R.	Trinity R.	Sacramento R.	San Joaquin R.
Snake R.	0.651	0.697	0.497	0.624	0.592
Yampa R.	0.554	0.409	0.504	0.588	0.647
Colorado R.	0.449	0.336	0.454	0.542	0.650
San Juan R.	*0.139*	*0.012*	*0.170*	*0.225*	0.363
lower CO tributaries	*0.054*	*-0.167*	*0.202*	*0.196*	0.404
PDSI-C. WA	0.596	0.523	0.497	0.520	0.494
PDSI-NE NV	0.539	0.330	0.486	0.595	0.696
Salinas R.	0.451	*0.264*	0.757	0.737	0.847
PDSI-S. CA	0.596	0.523	0.497	0.520	0.494

b. reconstructed	Klamath Falls	Klamath R.	Trinity R.	Sacramento R.	San Joaquin R.
Snake R.	0.394	0.340	0.614	0.618	0.550
Yampa R.	*0.179*	*0.190*	0.464	0.496	0.494
Colorado R.	*0.194*	*0.202*	0.505	0.533	0.549
San Juan R.	*0.011*	*-0.036*	*0.244*	0.307	0.381
Lower CO tribs.	*0.025*	*-0.147*	*0.219*	*0.252*	0.348
PDSI-C.WA	0.570	0.543	0.595	0.572	0.456
PDSI-NE NV	0.324	*0.256*	0.604	0.646	0.655
Salinas R.	0.369	*0.208*	0.676	0.719	0.821
PDSI-S.CA	0.310	*0.090*	0.565	0.632	0.721

Table 13. Correlations for reconstructed water year precipitation and streamflow for Klamath, Sacramento, and San Joaquin basins and other hydroclimatic reconstructions in the western US. For the full common period, a.1591-1997, and for b. 1600s, c. 1700s, d. 1800s, and e. 1900s to 1997. Red values are not significant at $p < 0.05$

a. 1591-1997	Klamath Falls	Klamath R.	Trinity R.	Sacramento R.	San Joaquin R.
Klamath Falls	1.000				
Klamath R.	0.589	1.000			
Trinity R.	0.581	0.476	1.000		
Sacramento R.	0.590	0.399	0.914	1.000	
San Joaquin R.	0.542	0.334	0.864	0.957	1.000
Snake R.	0.332	0.193	0.399	0.412	0.400
Yampa R.	0.128	*0.083*	0.205	0.283	0.315
Colorado R.	0.156	*0.065*	0.255	0.337	0.361
San Juan R.	0.152	*-0.008*	0.250	0.322	0.351
Lower CO tribs.	*0.092*	*-0.053*	0.207	0.261	0.303
PDSI-C.WA	0.582	0.385	0.475	0.488	0.420
PDSI-NE NV	0.373	0.221	0.503	0.588	0.590
Salinas R.	0.288	0.123	0.716	0.786	0.843
PDSI-S.CA	0.320	*0.088*	0.609	0.697	0.737

b. 1600-1699	Klamath Falls	Klamath R.	Trinity R.	Sacramento R.	San Joaquin R.
Klamath Falls	1.000				
Klamath R.	0.581	1.000			
Trinity R.	0.507	0.360	1.000		
Sacramento R.	0.538	0.295	0.877	1.000	
San Joaquin R.	0.493	0.223	0.808	0.953	1.000
Snake R.	0.336	*0.192*	0.257	0.266	0.254
Yampa R.	*0.169*	*0.135*	*0.179*	0.255	0.303
Colorado R.	*0.144*	*0.054*	*0.164*	0.258	0.270
San Juan R.	*0.170*	*0.020*	*0.189*	0.251	0.249
Lower CO tribs.	*0.136*	*0.006*	0.271	0.282	0.297
PDSI-C.WA	0.505	0.264	0.371	0.421	0.349
PDSI-NE NV	0.343	*0.179*	0.511	0.612	0.633
Salinas R.	0.220	*0.070*	0.685	0.787	0.837
PDSI-S.CA	0.247	*0.000*	0.571	0.697	0.736

c. 1700-1799	Klamath Falls	Klamath R.	Trinity R.	Sacramento R.	San Joaquin R.
Klamath Falls	1.000				
Klamath R.	0.621	1.000			
Trinity R.	0.498	0.426	1.000		
Sacramento R.	0.508	0.343	0.926	1.000	
San Joaquin R.	0.510	0.322	0.896	0.969	1.000
Snake R.	0.314	*0.069*	0.411	0.456	0.450
Yampa R.	0.228	*0.092*	0.277	0.418	0.386
Colorado R.	0.207	*0.066*	0.286	0.426	0.409
San Juan R.	0.201	*0.040*	0.312	0.449	0.441
Lower CO tribs.	*0.091*	*-0.038*	*0.194*	0.290	0.309
PDSI-C.WA	0.560	0.410	0.524	0.492	0.456
PDSI-NE NV	0.397	0.198	0.427	0.570	0.563
Salinas R.	0.276	*0.091*	0.765	0.843	0.864
PDSI-S.CA	0.302	*0.071*	0.569	0.703	0.722

d. 1800-1899	Klamath Falls	Klamath R.	Trinity R.	Sacramento R.	San Joaquin R.
Klamath Falls	1.000				
Klamath R.	0.470	1.000			
Trinity R.	0.629	0.331	1.000		
Sacramento R.	0.598	0.247	0.895	1.000	
San Joaquin R.	0.529	0.226	0.859	0.958	1.000
Snake R.	0.373	*0.168*	0.439	0.435	0.440
Yampa R.	*0.040*	*0.073*	*0.104*	*0.183*	0.253
Colorado R.	*0.135*	*0.035*	*0.191*	0.273	0.329
San Juan R.	*0.178*	*-0.046*	0.258	0.312	0.346
Lower CO tribs.	*0.110*	*-0.094*	*0.178*	0.248	0.283
PDSI-C.WA	0.636	0.312	0.441	0.455	0.421
PDSI-NE NV	0.394	0.214	0.504	0.550	0.552
Salinas R.	0.287	*-0.013*	0.701	0.783	0.846
PDSI-S.CA	0.405	*0.089*	0.727	0.761	0.775

e. 1900-1997	Klamath Falls	Klamath R.	Trinity R.	Sacramento R.	San Joaquin R.
Klamath Falls	1.000				
Klamath R.	0.682	1.000			
Trinity R.	0.710	0.719	1.000		
Sacramento R.	0.712	0.659	0.946	1.000	
San Joaquin R.	0.634	0.532	0.890	0.951	1.000
Snake R.	0.350	0.356	0.507	0.499	0.465
Yampa R.	*0.097*	*0.070*	0.297	0.317	0.348
Colorado R.	*0.171*	*0.153*	0.391	0.410	0.447
San Juan R.	*0.069*	*0.001*	0.268	0.298	0.386
Lower CO tribs.	*0.062*	*-0.101*	0.240	0.277	0.358
PDSI-C.WA	0.619	0.571	0.560	0.575	0.450
PDSI-NE NV	0.374	0.307	0.586	0.628	0.615
Salinas R.	0.383	0.291	0.714	0.742	0.832
PDSI-S.CA	0.356	0.205	0.615	0.660	0.730

Figures

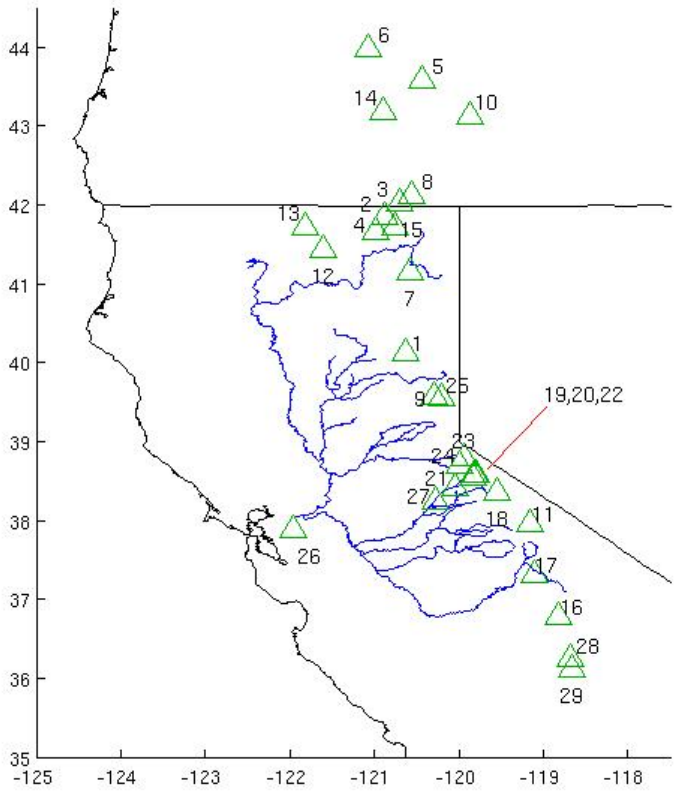

Figure 1. Map showing locations of the 29 tree-ring sites for field collections on this project. Species and other information on the sites are listed in Table1.

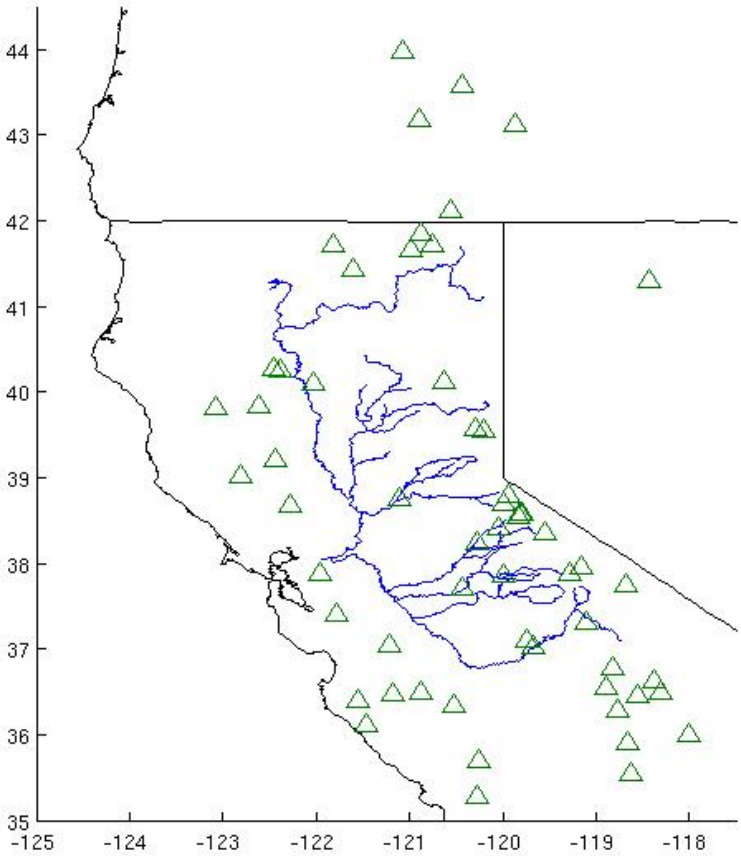

Figure 2. Map showing 6l-site tree-ring network for reconstruction modeling of Sacramento and San Joaquin River basins. Reconstruction of any flow record draws on a subset of these sites, whose names, site information, and basic chronology statistics are listed in Appendix C.

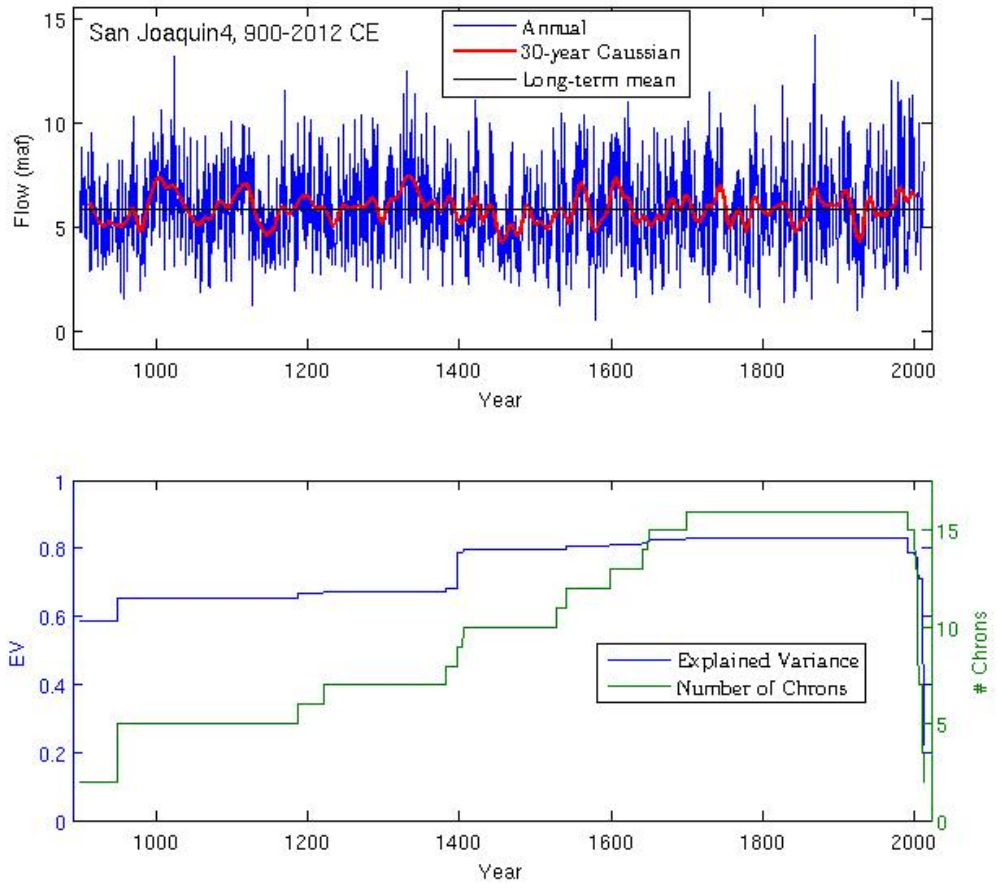

Figure 3. Reconstruction time series for San Joaquin River Runoff, 900-2012 CE. Top: annual and 30 yr Gaussian-smoothed reconstructed flow. Bottom: number of chronologies (N) in nested Loess model and decimal fraction of variance of flow explained (EV) by model.

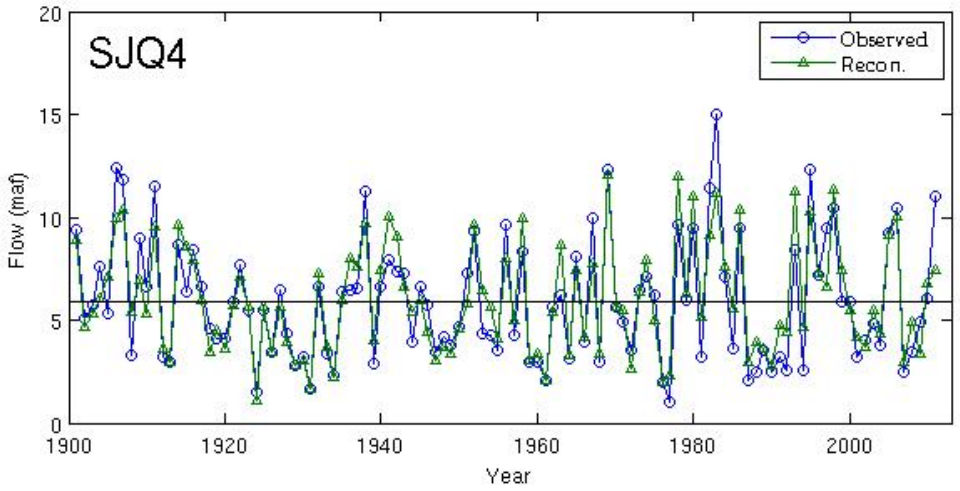

Figure 4. Time plots of observed and reconstructed flow, San Joaquin River Runoff, 1901-2011. Horizontal line at observed mean. For reconstruction statistics, see last line of Table 2.

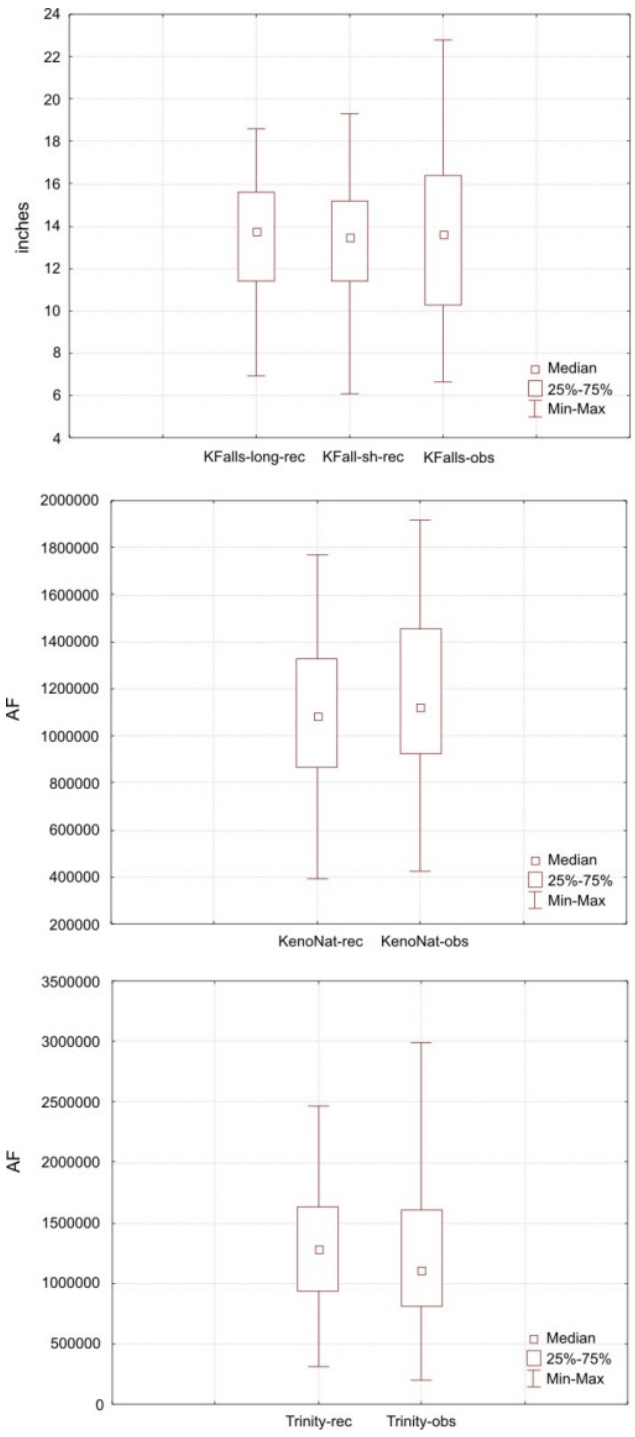

Figure **5**. Box plots for Klamath Falls water year precipitation (1912-2000), Klamath at Keno estimated natural water year flow (1949-2000), and Trinity River water year flow (1912-2000), reconstructions and observed series. Plots show median (center square) 25th and 75th percentiles (rectangle) and extreme high and low values. For the Klamath at Keno, results for the two reconstruction models are shown (one starting in 1000 and one in 1610).

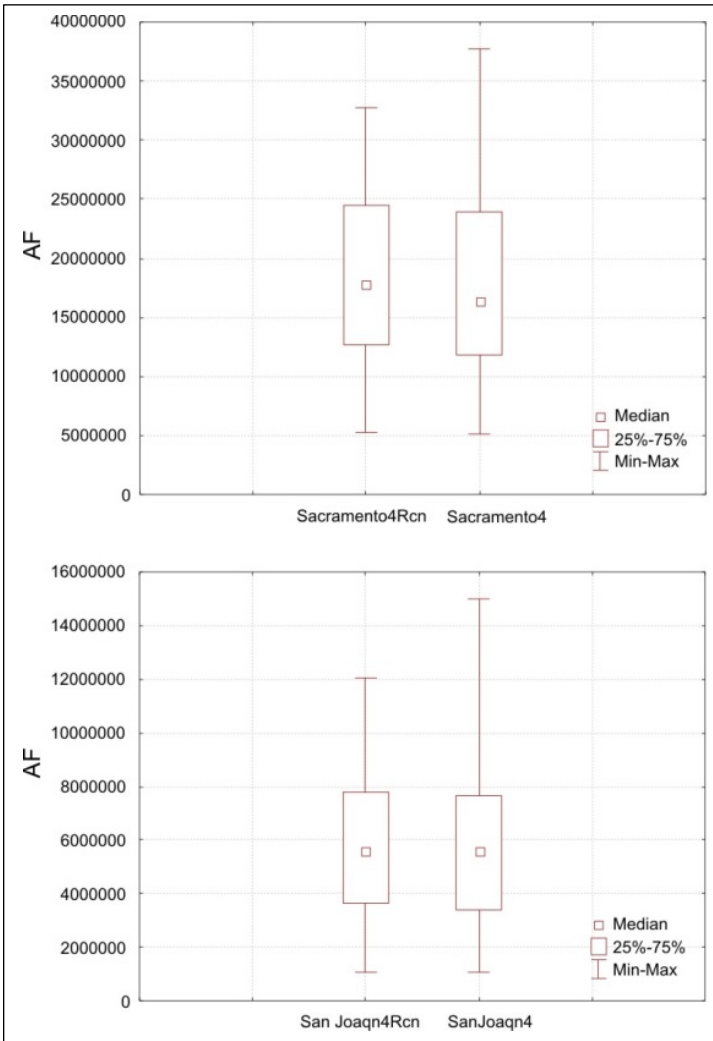

Figure 6. Box plots for Sacramento (4 rivers average) and San Joaquin (4 rivers averages) water streamflow, (1906-2011), reconstructions and observed series. Plots show median (center square) 25th and 75th percentiles (rectangle) and extreme high and low values.

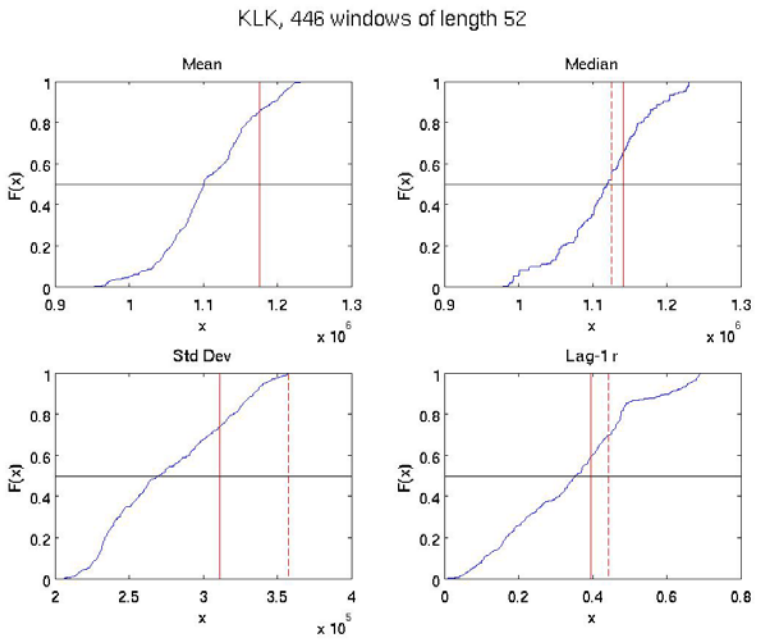

Figure 7. Cumulative distribution functions of hydrologic statistics in *m*-year overlapping windows offset by one year for Klamath River (KLK) flow reconstruction. Statistics, clockwise from upper right are mean, median, standard deviation and lag-1 autocorrelation. X-axis units are flow in acre-ft for first three statistics, and dimensionless for the last. Y-axis is non-exceedance probability of the statistic at given value of x. Vertical lines mark the value of the statistic for the reconstruction (solid) or observations (dashed) for the single *m*-year period of overlap of observed and reconstructed series. If only solid vertical line, the statistic is identical for the two series. Offset of vertical lines shows the bias in reproducing the calibration-period value of the statistic. For standard deviation this offset also reflects unexplained variance in the reconstruction. Annotated at top of figure are the number of windowed-periods and the length (years) of the window. For example, the 52-year overlap period of observed and reconstructed flows was relatively wet: the reconstructed sample mean for this period, about 1.15 million acre-feet, ranks near the 80th percentile of 446 sample means computed for a total of 446 overlapping 52-year periods.

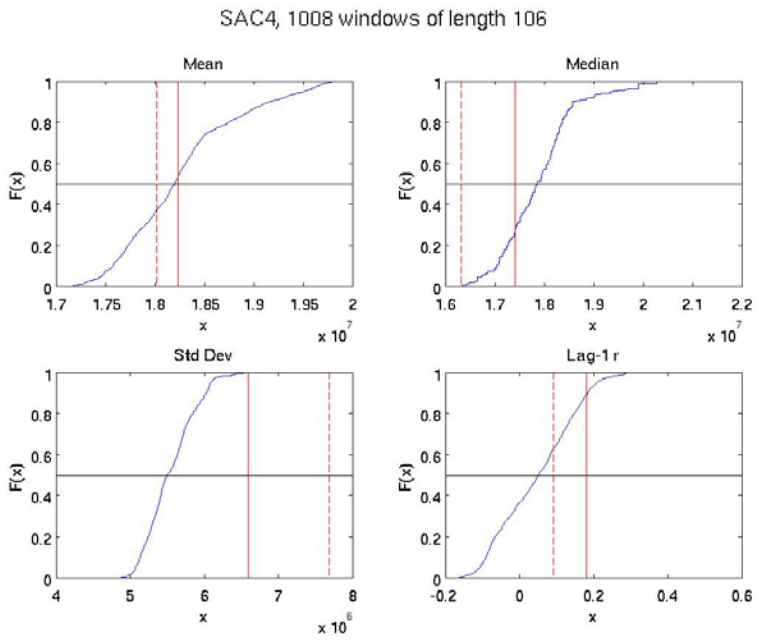

Figure 8. Cumulative distribution functions of hydrologic statistics in *m*-year overlapping windows offset by one year for long-term reconstruction of Sacramento (SAC4) reconstructed flows. Components of plots described in caption to Figure 7.

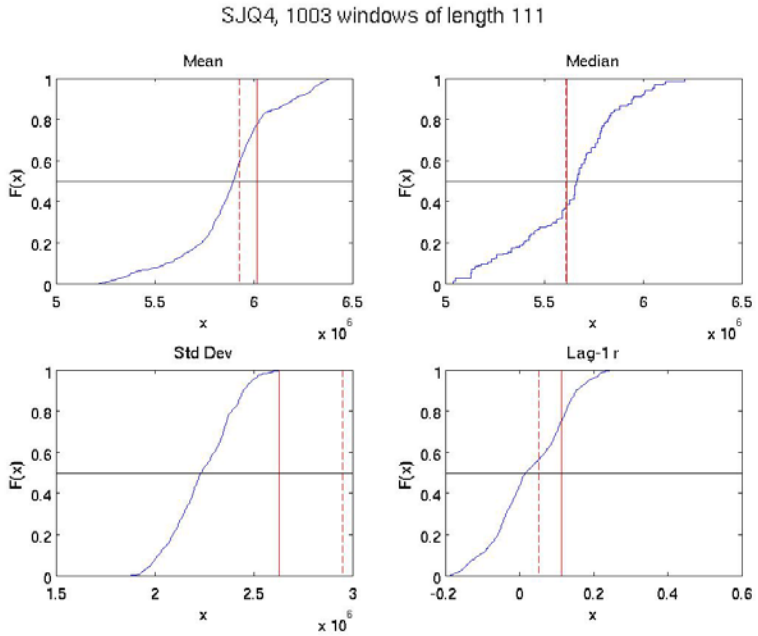

Figure 9. Cumulative distribution functions of hydrologic statistics in *m*-year overlapping windows offset by one year for long-term reconstruction of San Joaquin (SJQ4) reconstructed flows. Components of plots described in caption to Figure 7.

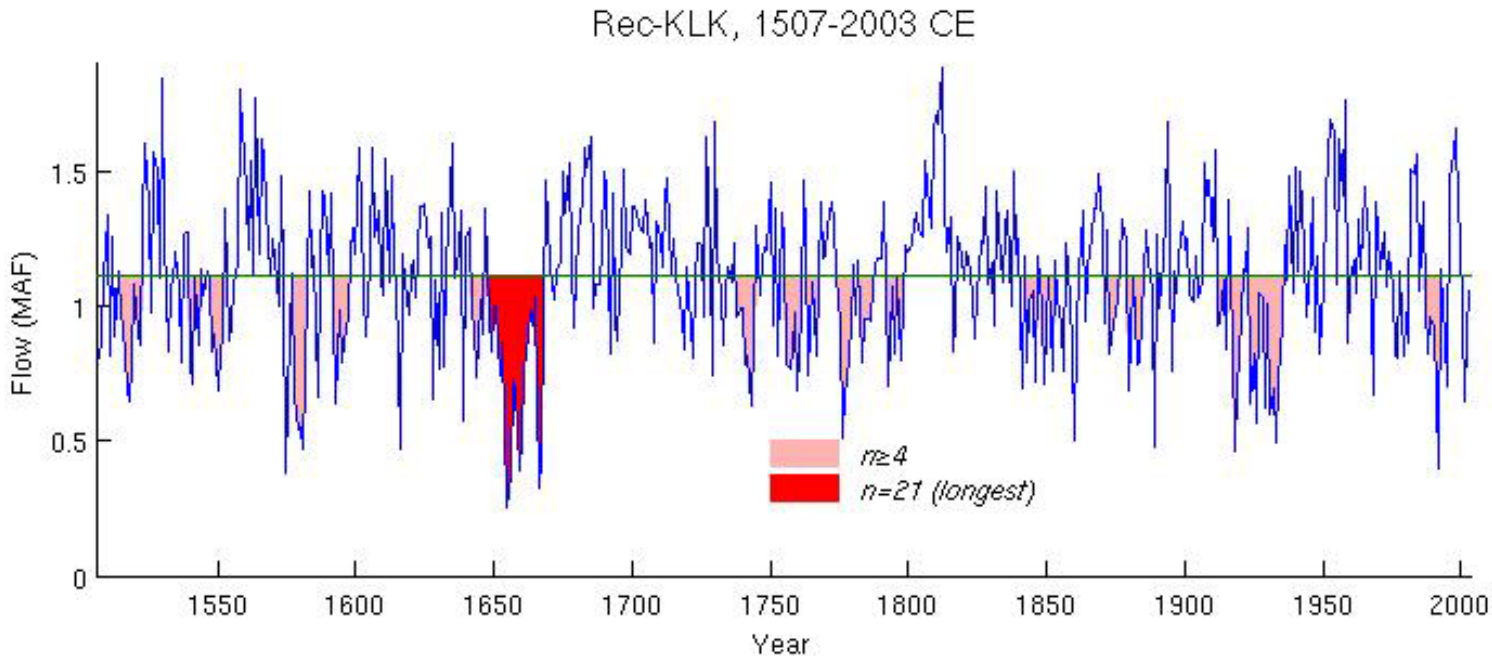

Figure 10. Reconstructed flows of Klamath River, 1507-2003. Horizontal line at median. Color-shading marks longest run and all other runs greater than specified length.

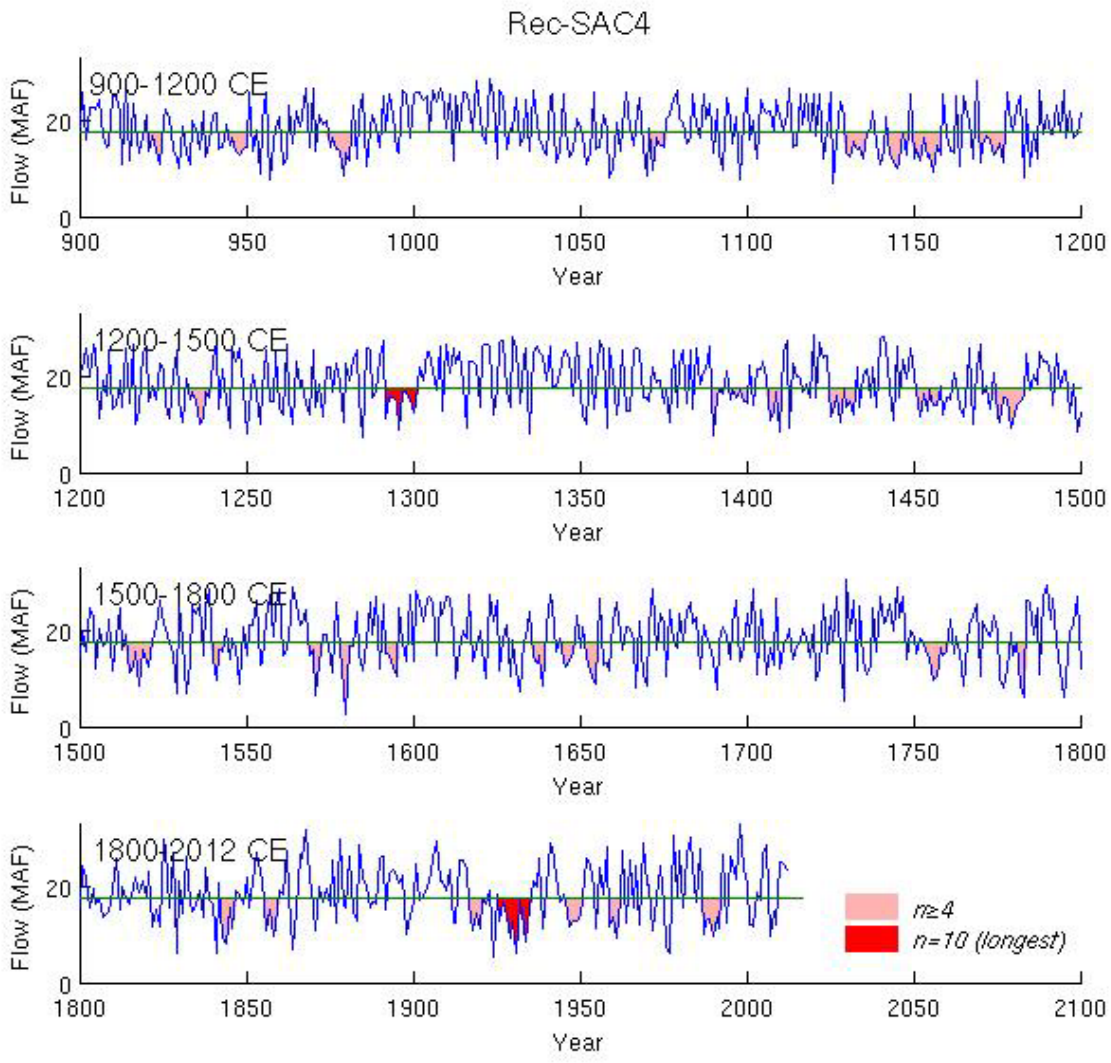

Figure 11. Reconstructed flows of Sacramento River (SAC4), 900-2010 CE. Horizontal line at median. Color-shading marks longest run and all other runs greater than specified length.

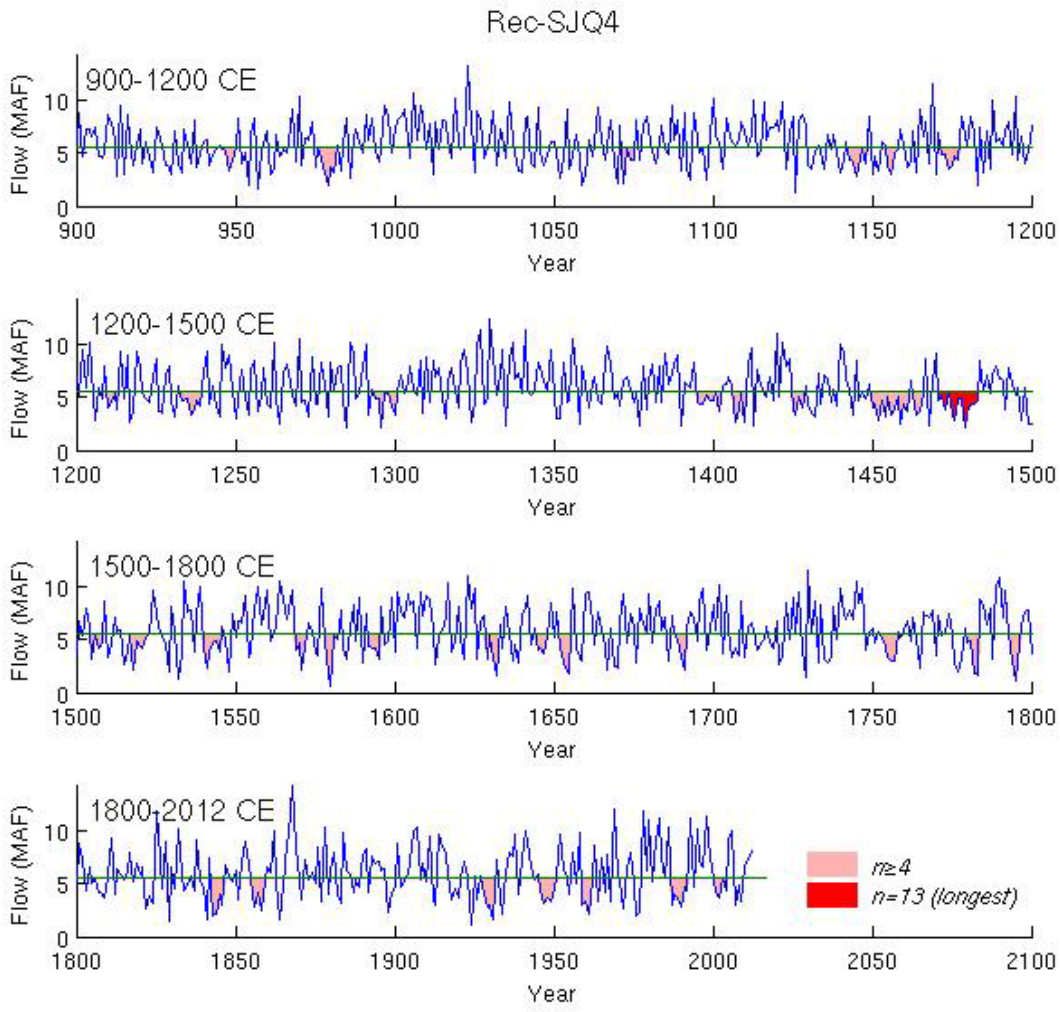

Figure 12. Reconstructed flows of San Joaquin River (SAC4), 900-2010 CE. Horizontal line at median. Color-shading marks longest run and all other runs greater than specified length.

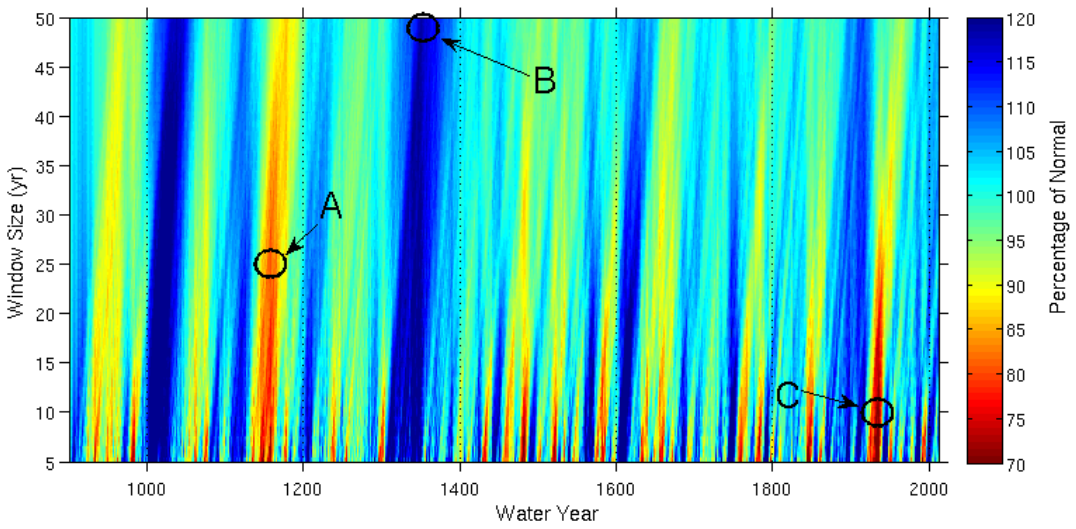

Figure 13. Color-mapped running means of reconstructed flows of Sacramento River (SAC4), 900-2012 CE. Anomaly in *m*-year moving-average flow, where *m* is the window size, is color-coded as percentage of long-term normal observed flow. Time axis (x axis) is ending year of the *m*-year window. Key at right associates colors with flow anomaly – lower flow toward red and higher flows toward blue. Any *m*-year flows lower than 70% or higher than 120% of mean are assigned same color as 70% and 120%. For example, arrow A marks a period in the 1100s (x axis) with 25-yr means (y axis) less than 85% of long-term mean (color key at right). Similarly, arrow B marks a 50-yr period ending in mid-1300s with unmatched wetness (more than 120% of long-term mean), and arrow C highlights the unprecedented dryness of the 1930s in terms of low ten-year-mean flow.

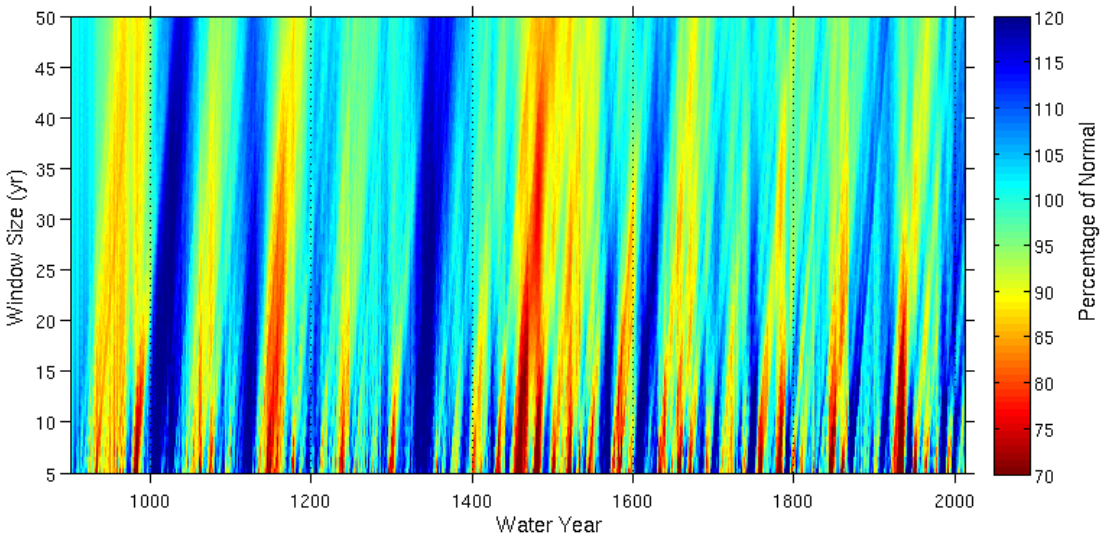

Figure 14. Color-mapped running means of reconstructed flows of San Joaquin River (SJQ4), 900-2012 CE. Interpretation of colors explained in caption for Figure 13.

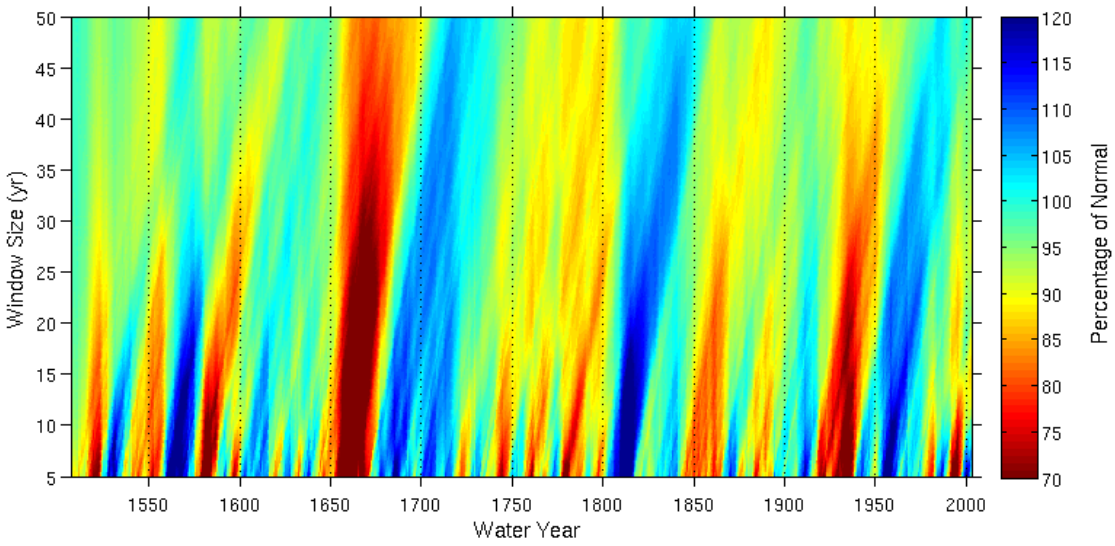

Figure 15. Color-mapped running means of reconstructed flows of Klamath River (KLK), 1507-2003 CE. Interpretation of colors explained in caption for Figure 13.

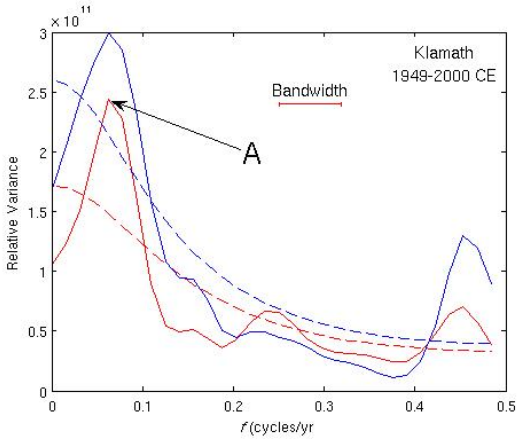

Figure 16. Spectra of observed (blue) and reconstructed (red) Klamath flows for calibration period. Red noise background dashed. Difference in total areas under spectrum reflects variance unexplained by tree rings. Spectra by smoothed periodogram method. Highest peak at frequency f=0.0625, which corresponds to a wavelength of about 16 years (annotated peak A).

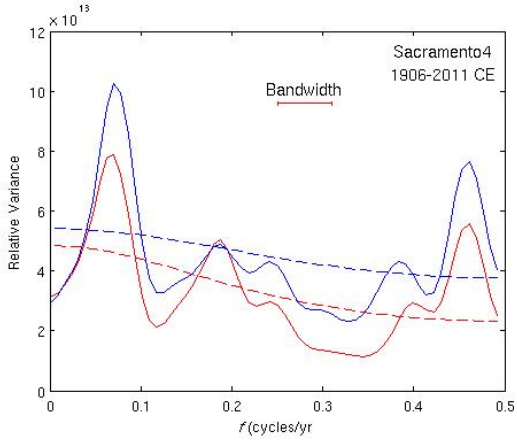

Figure 17. Spectra of observed (blue) and reconstructed (red) Sacramento4 flows for calibration period. Highest peak at wavelength of about 14 years. Remainder of caption as in Figure 16.

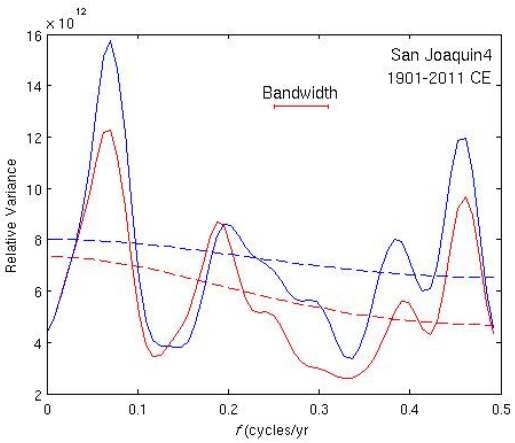

Figure 18. Spectra of observed (blue) and reconstructed (red) San Joaquin4 flows for calibration period. Highest peak at wavelength of about 14 years. Remainder of caption as in Figure 16.

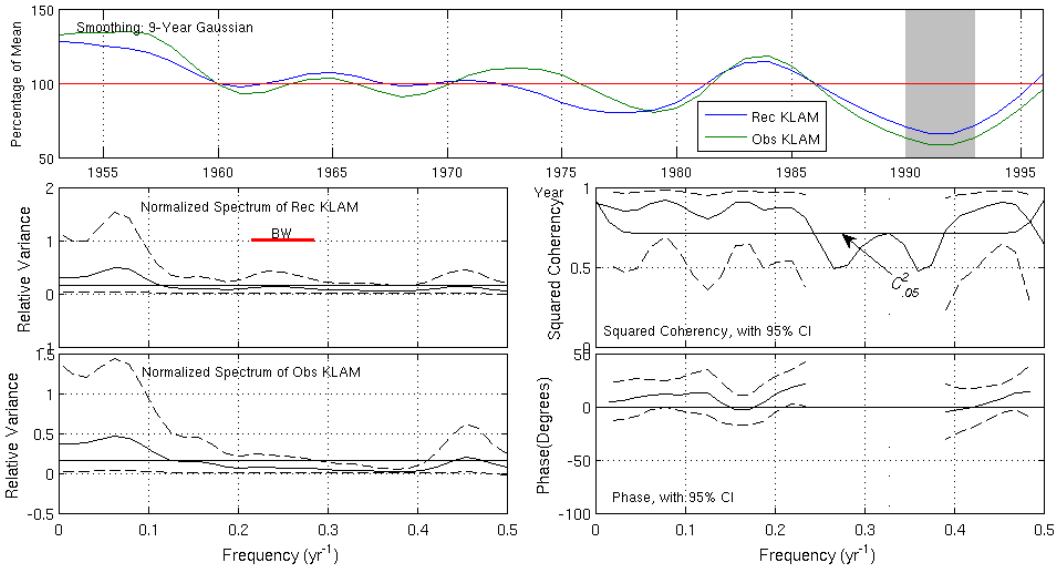

Figure 19. Smoothed time series and cross-spectral output for Klamath River. Analysis for overlap period of reconstructed and observed flows, 1949-2000. Top: Gaussian smoothed reconstructed and observed flow as percentage of mean. Left bottom two: normalized spectra of reconstructed and observed flows with 95% confidence interval. Right bottom two: squared coherency and phase series describing frequency properties of covariation of reconstructed and observed flows. Shading in top plots marks period both smoothed series in driest decile. Gaussian filter weights for smoothing the annual flows to produce the time series at top are as follows: [0.0135 0.0477 0.1172 0.2012 0.2408 0.2012 0.1172 0.0477 0.0135].

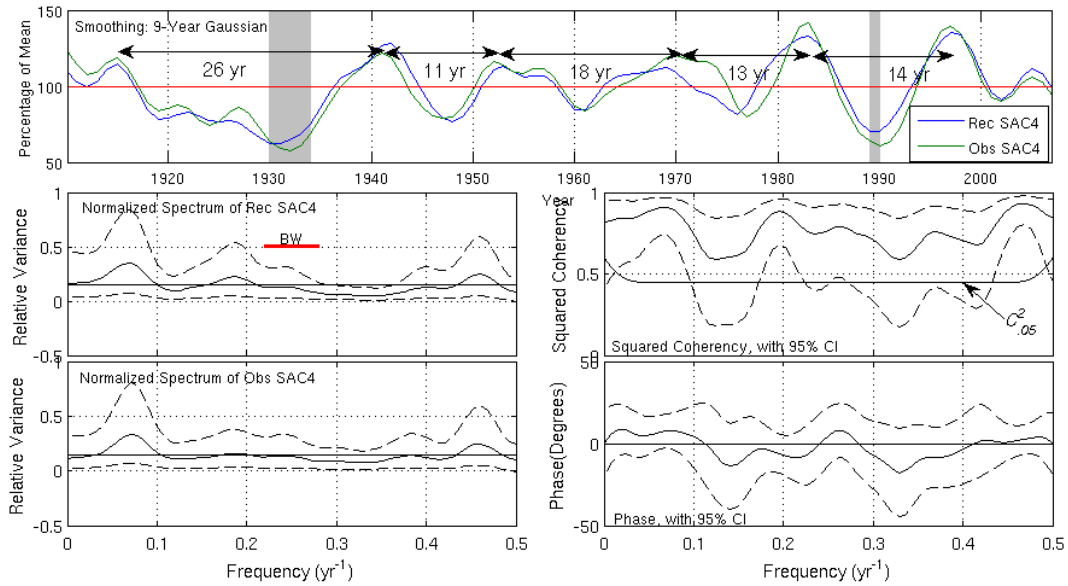

Figure 20. Smoothed time series and cross-spectral output for Sacramento River (SAC4). Analysis for overlap period of reconstructed and observed flows, 1906-2012. Double arrows (top) mark approximate intervals between peaks in smoothed flows. Average interval is 16.4 yr. Remainder of caption as in Figure 19.

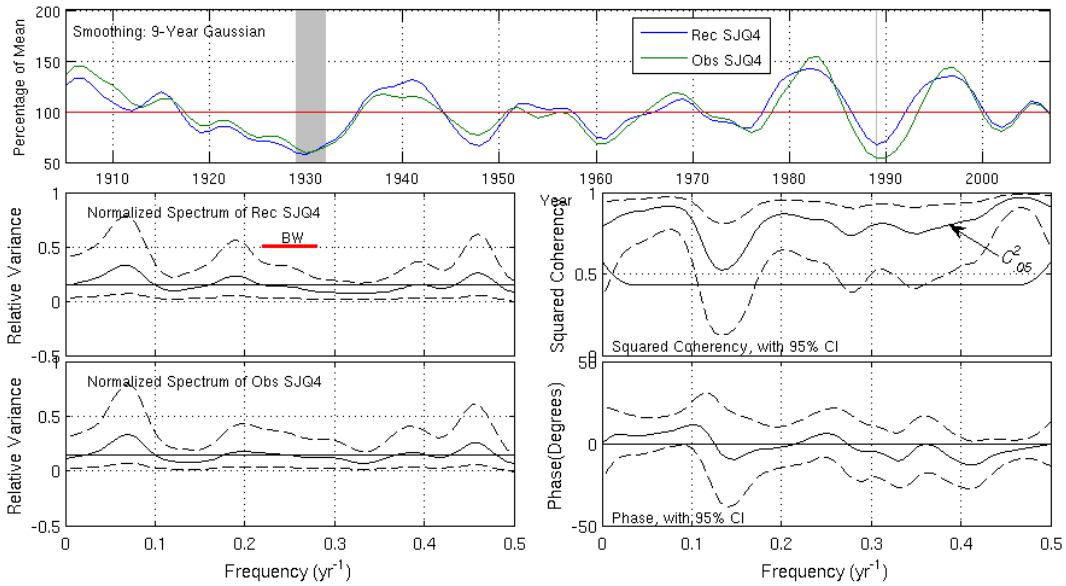

Figure 21. Smoothed time series and cross-spectral output for San Joaquin River (SJQ4). Analysis for overlap period of reconstructed and observed flows, 1901-2012. Remainder of caption as in Figure 19.

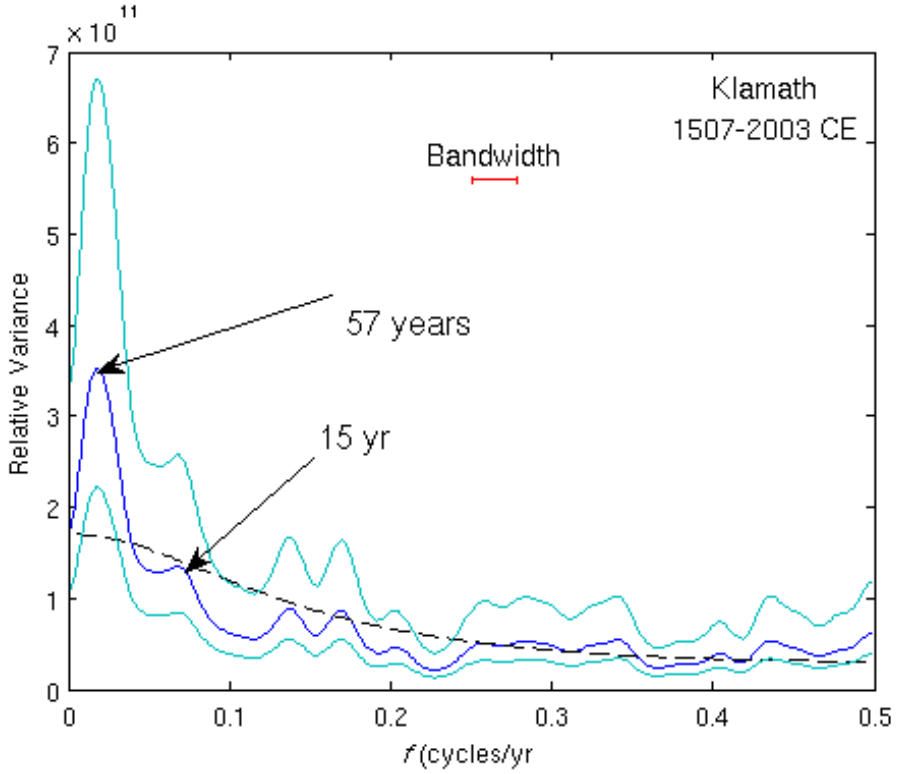

Figure 22. Spectrum with 95% confidence interval and red-noise null continuum for long-term reconstruction of Klamath reconstructed flows. Period of analysis and bandwidth for smoothed-periodogram spectrum annotated. Major peak is at 57 years. Next low-frequency peak is at 15 years. The null hypothesis of a red noise spectrum is rejected at a *p*-value of 0.05 (95% significance) only if the red noise spectrum (dashed line) falls outside the indicated confidence interval (light blue) around the estimated spectrum (dark blue).The spectal peak at 57 years is the only peak significantly different from a red noise spectrum.

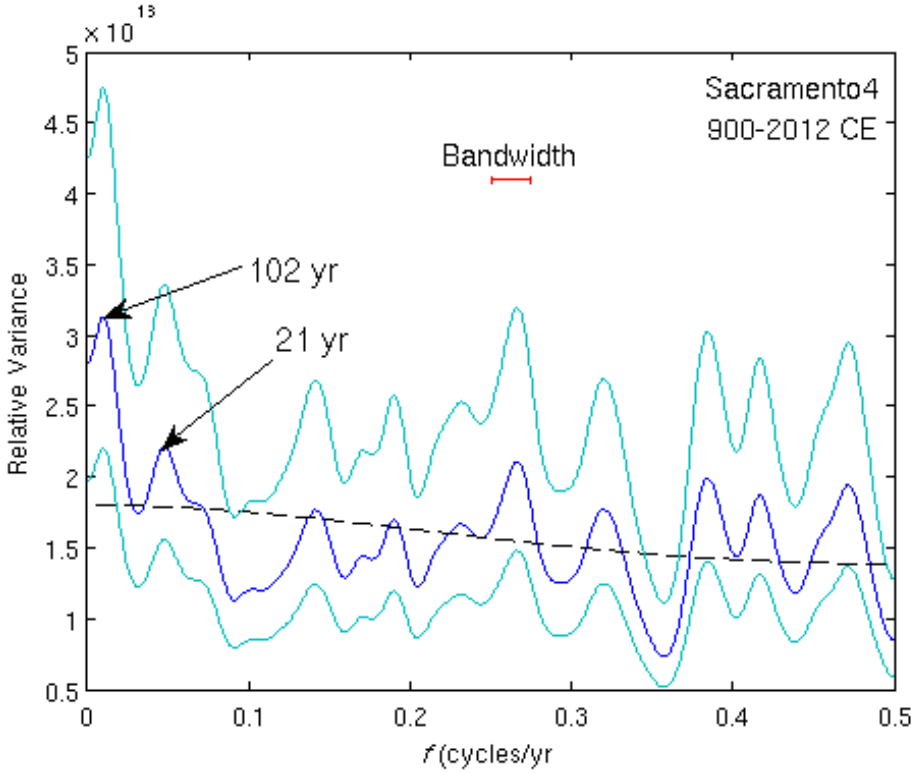

Figure 23. Spectrum with 95% confidence interval and red-noise null continuum for long-term reconstruction of Sacramento (SAC4) reconstructed flows. Period of analysis and bandwidth for smoothed-periodogram spectrum annotated. Major spectral peak is at 102 years, and secondary peak at 21 years. Only the major peaks differs significantly from red noise (dashed line). See caption of Figure 22 for how significance is judged.

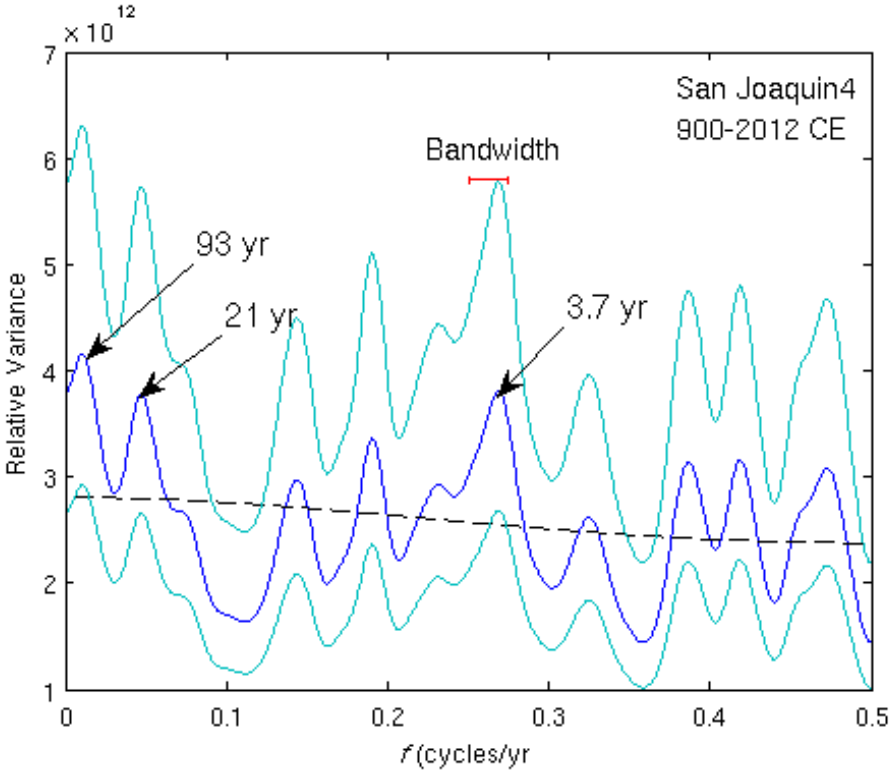

Figure 24. Spectrum with 95% confidence interval and red-noise null continuum for long-term reconstruction of San Joaquin (SJQ4) reconstructed flows. Period of analysis and bandwidth for smoothed-periodogram spectrum annotated. Major spectral peak is at 93 years. Second highest peak is at 3.7 years, and third highest at 21 years. Only the peak at 93 years and 3.7 years are significantly different (barely) from the red noise spectrum . See caption of Figure 22 for how significance is judged.

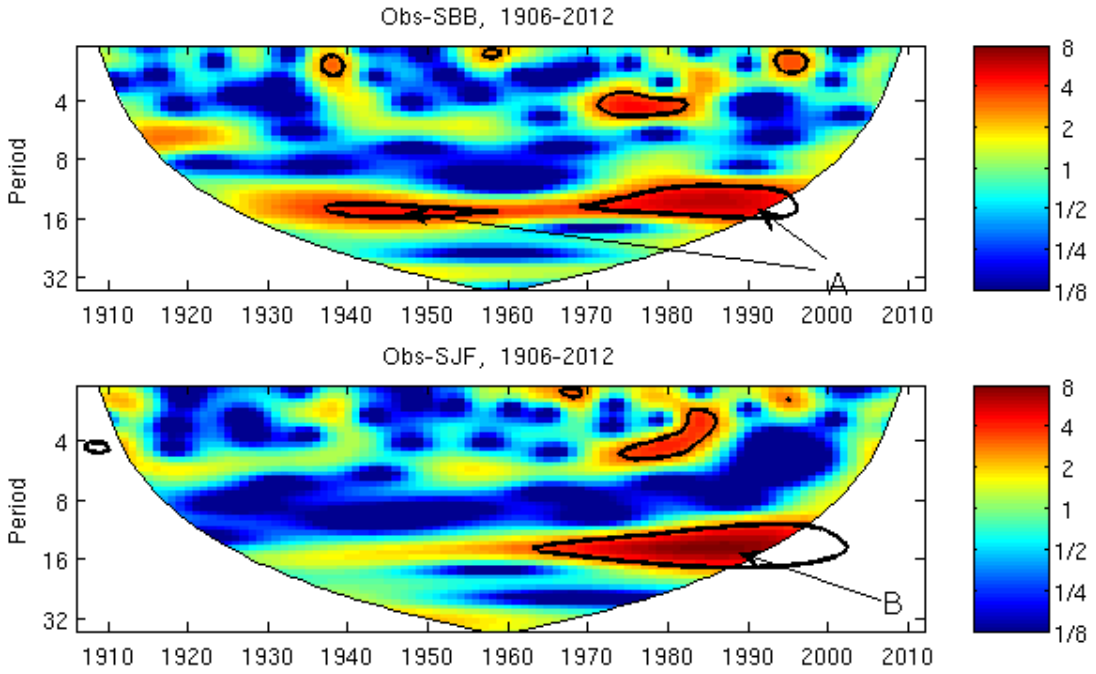

Figure 25. Continuous wavelet transforms(CWT) of observed flows of Sacramento River at Bend Bridge (SBB) and San Joaquin River inflow to Millerton Reservoir (SJF) , 1906-2012. These are the two most widely separated watersheds in the study for which we have millennial-length reconstructions. Color scale at right codes relative variance, with darkest red indicating 8 times the variance as blue-green (#1), and darkest blue indicating 1/8 the variance of blue-green. Thick black line delineates areas with variance significantly greater than expected for red noise at 95% confidence. Period on y axis at left is in years. The cone of influence (COI), the area in white outside the vase shaped region, marks parts of time-frequency space in which edge effects might distort the picture. Central year of period for which a particular color applies is given along the x axis. Spectra show high variance near a wavelength of 15 years throughout the observed record for SBB (arrow A), and in the most recent decades for SJF (arrow B).

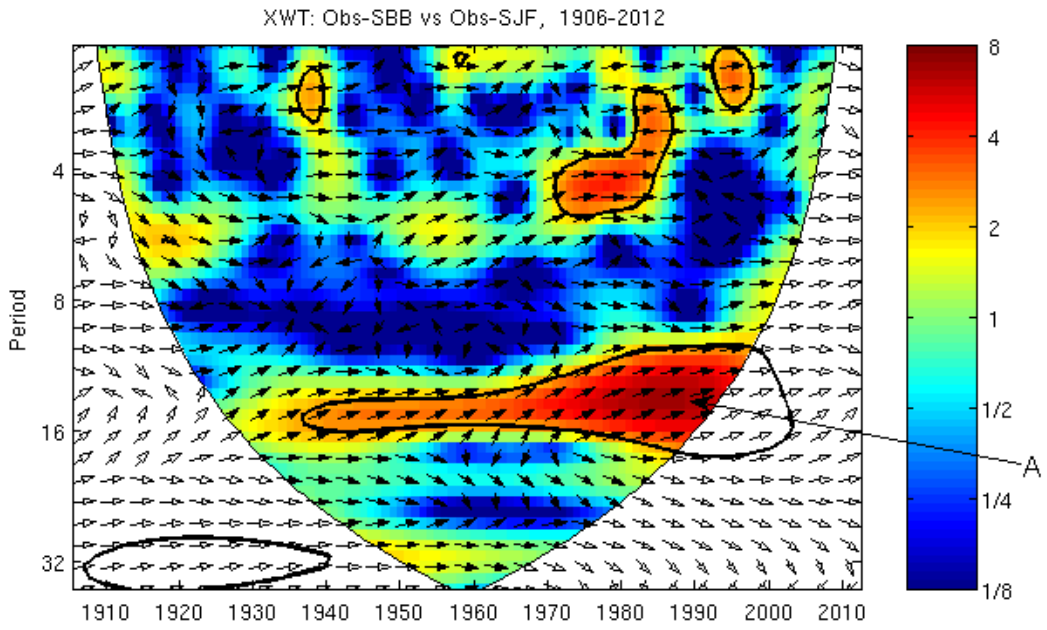

Figure 26. Cross wavelet transform (XWT) of observed flows of Sacramento River at Bend Bridge (SBB) and San Joaquin River inflow to Millerton Reservoir (SJF) , 1906-2012. Colors on the XWT code areas in time-frequency space in which variance is high in both series. Red indicates high variance, and blue indicates low variance. Thick black line indicated areas with significant (95%) common variance. The cone of influence (COI), the area in white outside the vase shaped region, marks parts of time-frequency space in which edge effects might distort the picture. Direction of arrows indicates phase relationship of variations: 0° (arrow to right) is perfectly in phase; 180° (arrow to left) is opposite phase, or peaks opposite troughs. Number of years of offset corresponding to a specific phase angle depends on the period in years (y axis). For example, at period of 15 years, 180°, or opposite phase, is an offset of 7.5 years, while for a period of 32 years, opposite phase is an offset of 16 years. Red region marked with arrow A indicates period when SBB and SJF both have much power (high variance) at wavelengths near 15 years. This high common high variance is concentrated toward the latter part of the observed record. For example, the arrow points to a period centered on about 1990. At wavelengths or periods near 15 years, the black arrows have an angle from the horizontal of about 30°. Near wavelength 15 years, 180° corresponds to an offset of 7.5 years, and 30° corresponds to an offset of only about a year. The 15-year fluctuations in SBB and SJF can therefore be considered approximately in phase. That the arrows on this band near a period of 15 years have about the same angle across the plot from the start to the end of the record (left to right) indicates the variations near that period are phase-locked through time.

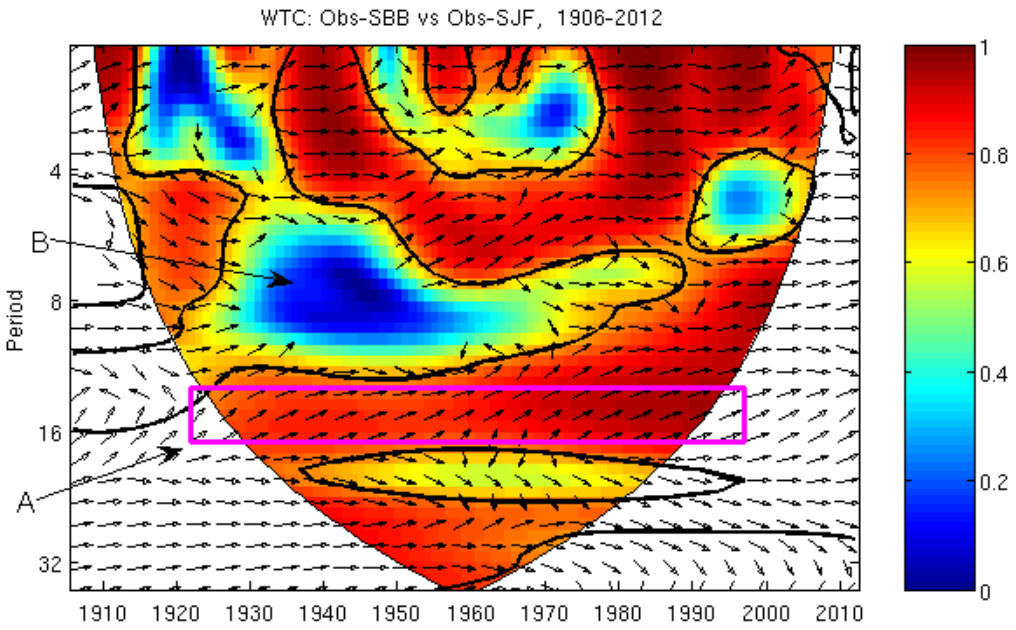

Figure 27. Wavelet coherence (WTC) between observed flows of Sacramento River at Bend Bridge (SBB) and San Joaquin River inflow to Millerton Reservoir (SJF) , 1906-2012. The WTC is analogous to correlation between two series as a function of time and frequency. The cone of influence (COI), the area in white outside the vase shaped region, marks parts of time-frequency space in which edge effects might distort the picture. The thick black line delineates areas with Monte Carlo significance of coherence at 95% or greater. Arrows indicate phase of relationship: arrow to right, perfectly in-phase (0 degrees); arrow to left, perfectly out of phase (180 degrees), or troughs at that wavelength in one series timed with peaks in the other (see caption for Figure 26). For these two series, coherence is significant over most of the figure. Area of low coherence (blue) coincides with periods with low variance at the indicated wavelength (Figure 25). A belt of in-phase significant coherence extends through the time series near the 15-year wavelength (arrow A). A region of low coherence, centered near 1945 and wavelength 8 years is marked by arrow B. Such a feature can be explained by the low variance in the individual series at that time (Figure 26).

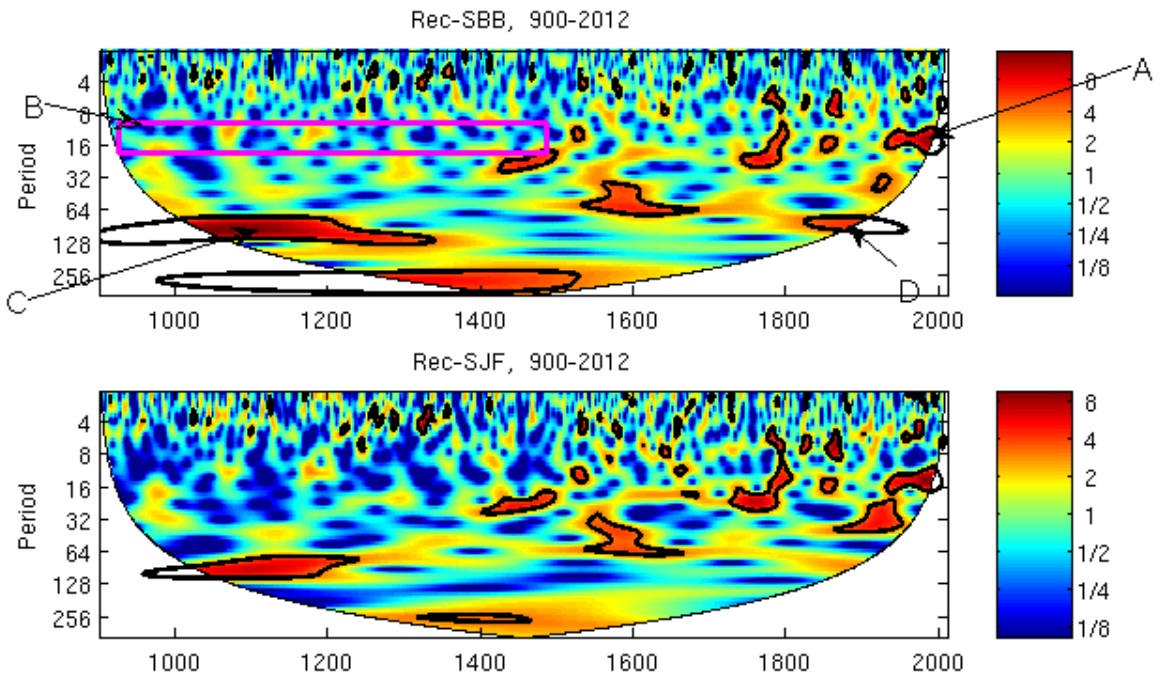

Figure 28. Continuous wavelet transforms (CWT) of reconstructed flows of Sacramento River at Bend Bridge (SBB) and San Joaquin River inflow to Millerton Reservoir (SJF) , 900-2012 CE. For interpretation of colors, axes, etc., refer to caption for Figure 25, which has plots for the observed flows. CWT for these reconstructions show that the high variance near a wavelength of 15 years that was evident in the much shorter records of observed flows is not consistent over centuries. The strongest evidence for cyclic behavior near wavelength 15 years is restricted to the period beginning in the 20th century (arrow A on plot for SBB). For a long stretch of time from the beginning of record till about 1500 CE, evidence of high variance near the 15-year wavelength is completely lacking (arrow B). The early part of the reconstruction shows cyclic behavior at very long wavelengths; such behavior is not consistent through the long reconstruction but does appear again until the 19th century (arrows C and D).

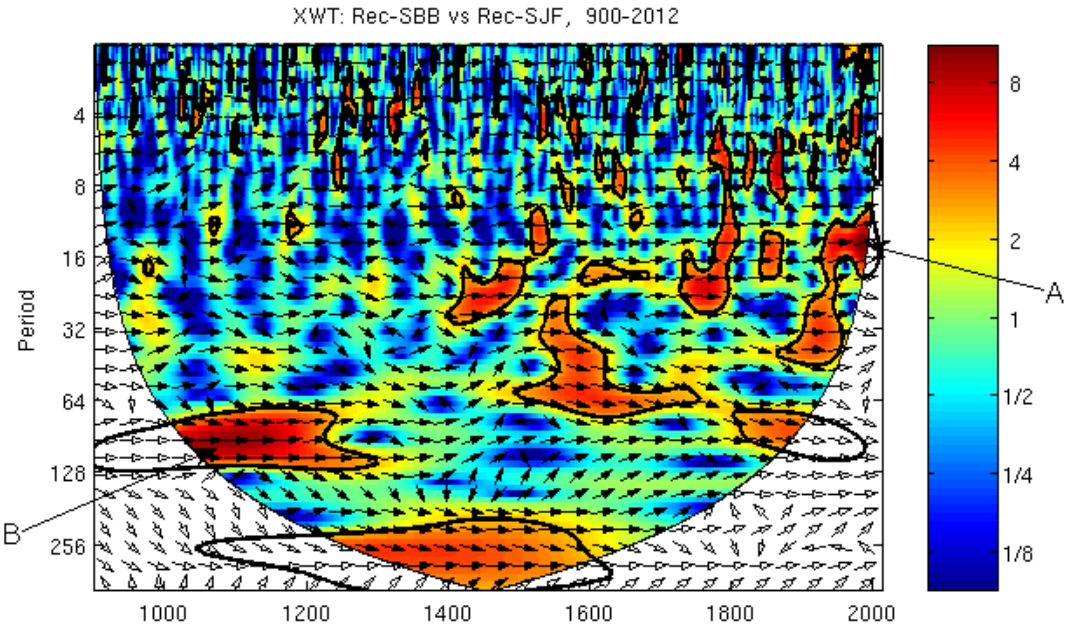

Figure 29. Cross wavelet transform (XWT) of reconstructed flows of Sacramento River River at Bend Bridge (SBB) and San Joaquin River inflow to Millerton Reservoir (SJF) , 900-2012 CE. For general interpretation of XWT features, see caption for figure 26. The XWT indicates when two series have high variance in particular wavelength-ranges, and if the variations at a particular frequency are in phase or not (arrows). This XWT shows that the high common variance in SBB and SJF near wavelength 15 years is present mainly in the 20th century (arrow A). Variance is high and in-phase in both series near a wavelength of 100 years prior to 1200 (arrow B).

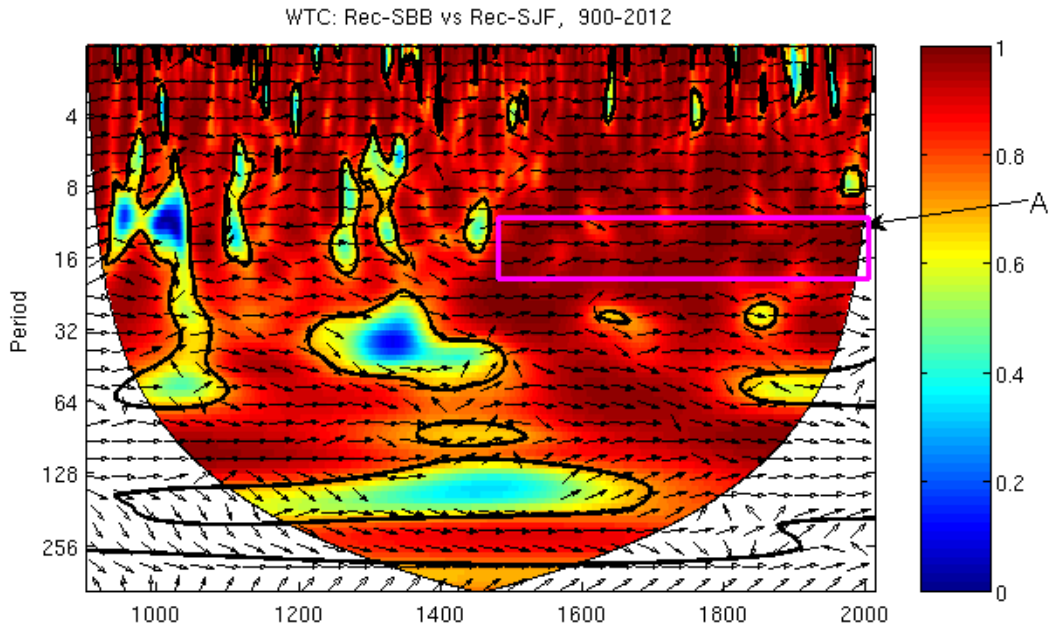

Figure 30. Wavelet coherence (WTC) between reconstructed flows of Sacramento River at Bend Bridge (SBB) and San Joaquin River inflow to Millerton Reservoir (SJF), 900-2012. Black line delineates Monte Carlo significance of coherence at 95%. See caption to Figure 27 for general point on interpretation of WTC. Coherence between these two reconstructions is significant over most of the time-frequency mapped in this figure (small areas of non-significant coherence are blue). A belt of high coherence and in-phase variations near wavelength of 15-25 years extends from present back to about 1500 (arrow A and purple box), but disappears in earlier centuries. Wavelength of strongest

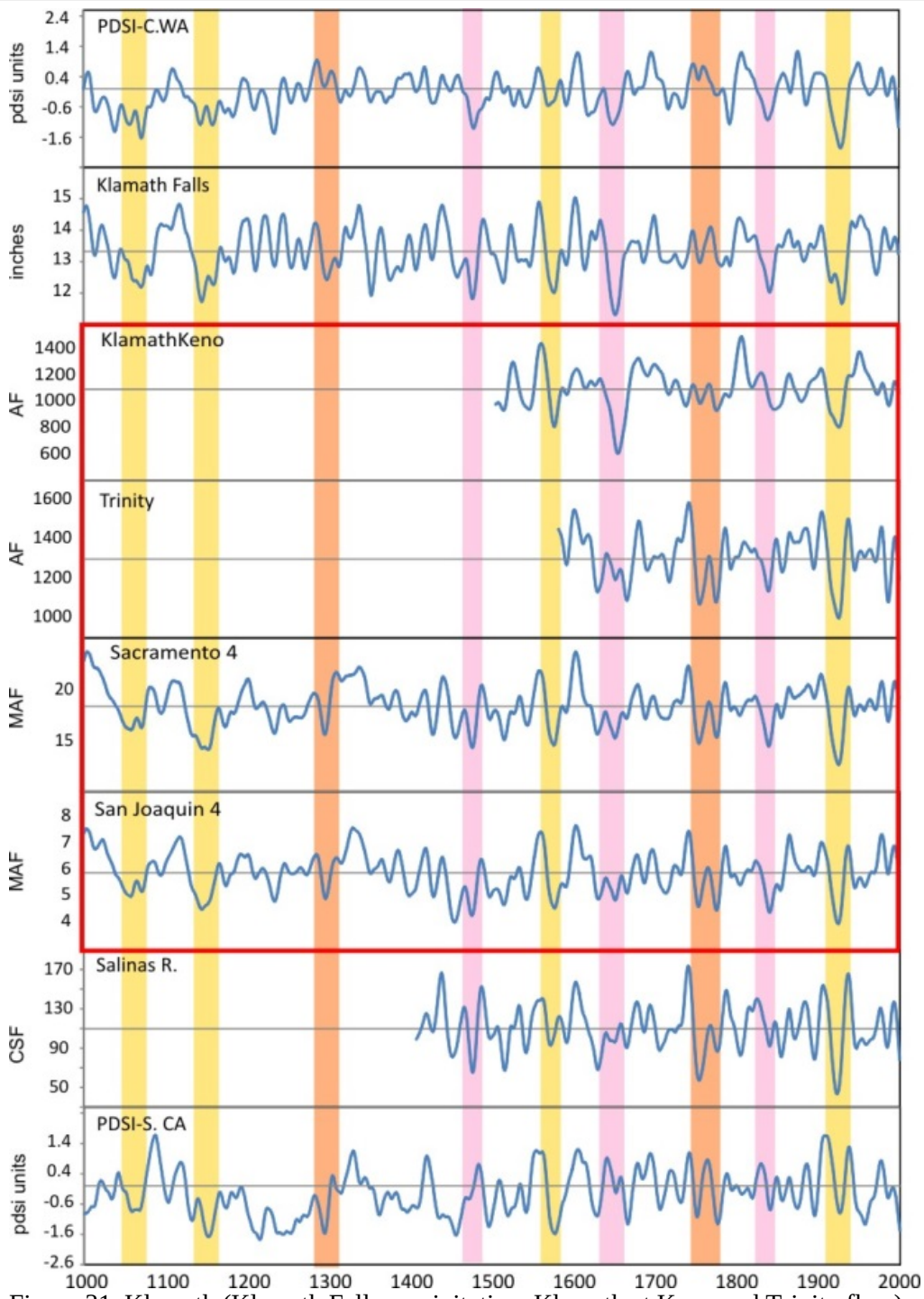

Figure 31. Klamath (Klamath Falls precipitation, Klamath at Keno and Trinity flow), Sacramento (4 rivers average), and San Joaquin (4 rivers average) with other western hydroclimate reconstructions, smoothed with a 20 year spline. Series are arranged from north to south. Major region-wide droughts are indicated with yellow bars, dry south-wet north are orange, and dry north-wet south are pink. Start dates are variable, all end in 2003.

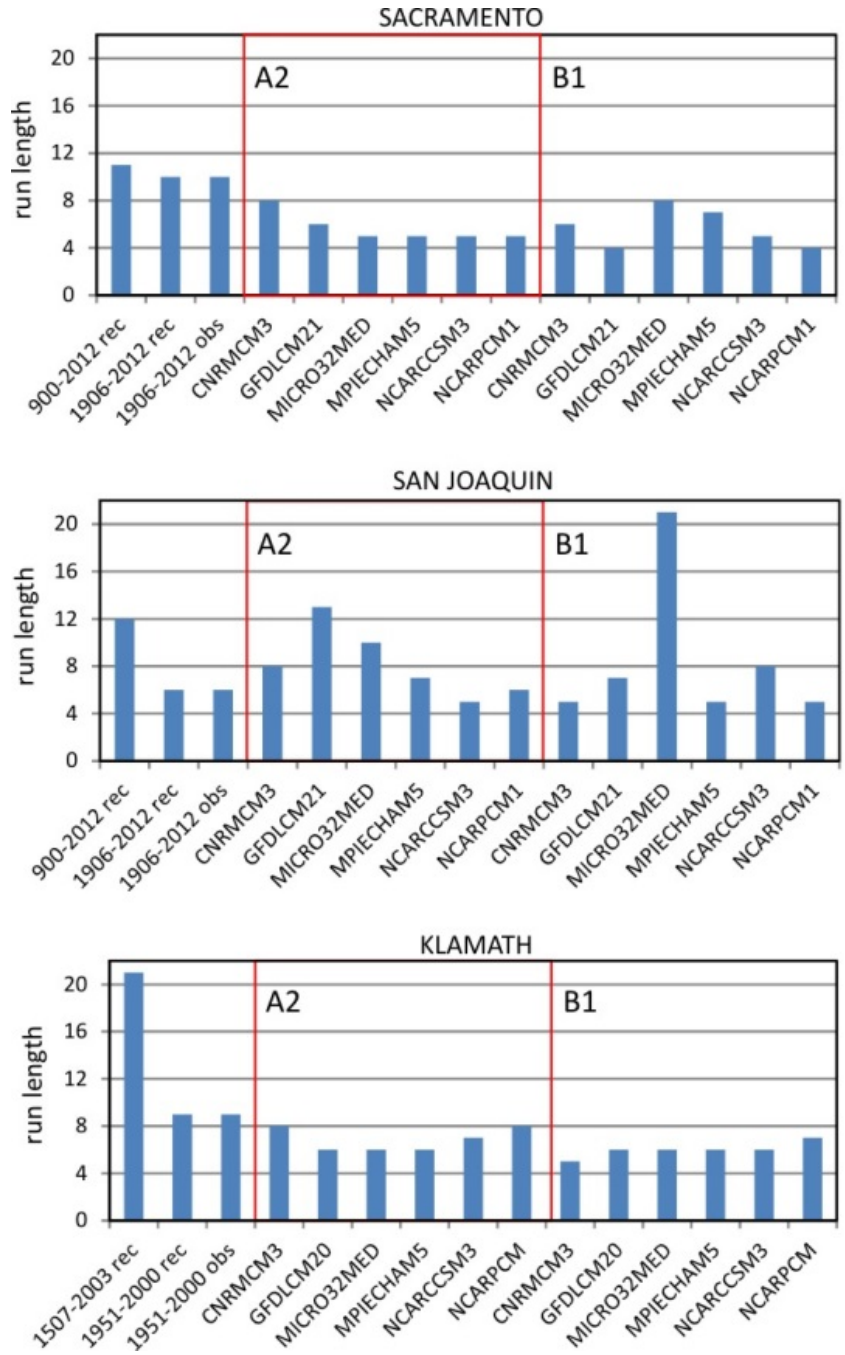

Figure 32. Maximum runs of drought years for Sacramento (top), San Joaquin (middle), and Klamath (bottom) flows; reconstructed (full and instrumental periods), observed series, and projected flows from a variety of downscaled GCMs for A2 and B1 scenarios, water years 1950-2099 (1951 start for Klamath).